Stage de recherche - FIP M1
École normale supérieure (Paris)

February - July, 2007

Marc Santolini

Estimation de paramètres cosmologiques par corrélation croisée d'observations de galaxies et du fond de rayonnement cosmologique

-

Estimating cosmological parameters through cross-correlation of galaxy surveys and Cosmic Microwave Background fluctuations

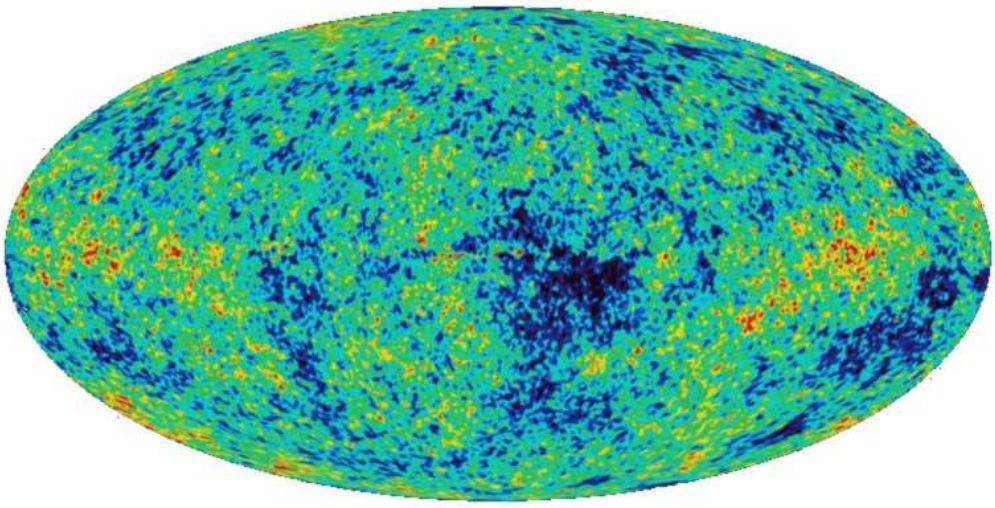

Supervisor: Prof. David N. Spergel

Department of Astrophysical Sciences
Princeton University, Princeton, NJ 08544 (USA)

Résumé

Au cours de la dernière décennie, l'étude de plus en plus précise du fond de rayonnement cosmologique (CMB), relique des âges obscurs qui ont suivi le Big-Bang, a permis une profonde amélioration de la connaissance de l'univers dans lequel nous vivons, de sa composition et de son histoire. Tous ces éléments sont résumés en quelques simples paramètres, les ***paramètres cosmologiques****. En comparant les observations à des prédictions théoriques, il est possible de trouver la valeur de ces paramètres, à une erreur près qui tient à l'imprécision de l'observation : c'est là l'objet de la contrainte de paramètres. Les observations à venir semblent prometteuses quant à la précision atteignable, et il est d'ores et déjà possible de prédire une amélioration conséquente dans notre estimation des paramètres. L'utilisation de corrélations croisées entre différents types d'observations permet de plus l'obtention d'informations sous-jacentes qui permettent de nouvelles contraintes. En modélisant une observation de galaxies, qui sont supposées être des points de repère visibles des surdensités de la mystérieuse et invisible matière noire, principale composante de la matière dans l'univers, et une observation du CMB, dont l'image est déformée par effet de lentille gravitationelle causé par cette même matière noire, nous pouvons déduire des corrélations entre les deux signaux de riches informations non seulement sur la matière noire, mais aussi sur l'énergie sombre, autre composante encore mal comprise de notre univers. Notre étude se base sur deux observations à venir : PLANCK pour le CMB et ADEPT pour l'observation de galaxies. La généralité du code que nous avons écrit permet en fait d'adapter cette étude à tout type d'observation. Je présente dans ce rapport de stage ce travail de contrainte de paramètres cosmologiques réalisé avec David Spergel, directeur du département de Sciences Astrophysiques de Princeton.*

Summary

The past decade has seen a dramatic improvement in our understanding of the Universe, of its composition, and its history, through the ever more precise observation of the Cosmic Microwave Background (CMB), a snapshot of what the Universe looked like shortly after the Big-Bang. This knowledge is described by only a few parameters, the so-called ***cosmological parameters****. Comparing the observations to theoretical predictions allows us to extract the values of these parameters with a confidence that depends on how noisy our experiments are: this is the parameters constraint. Future galaxy surveys and CMB observations will have better instruments that should reach high precision. Combining these observations through the use of cross-correlations should bring new insights on what cosmological parameters are. Modeling a galaxy survey, whose observed galaxies are supposed to be tracers of the underlying dark matter, and a CMB observation, which is modified with respect to the true emitted CMB because of the gravitational lensing photons experience around that same foreground dark matter, we show that we can extract precious information on dark matter as well as dark energy, the two most mysterious but major components of our Universe. Here, we predict how good such constraints could be using the specifications of two upcoming experiments: PLANCK for the CMB and ADEPT for the galaxy survey. The generality of the code we developped actually allows us to adapt our study to any kind of survey. The present report summarizes the work on cosmological parameters constraint I realized with David Spergel, chair of the Department of Astrophysical Sciences at Princeton University.*

Acknowledgements

I would like to genuinely thank Prof. David Spergel for welcoming me in his group and for the very interesting work he suggested to me; Aurélien Fraisse, former ENS student and now second year graduate student in the group, for his help to prepare my arrival in Princeton, his availability to recommend introductory readings about cosmology and to answer my questions about programming; Sudeep Das, third year graduate student in the group, for answering the numerous questions I had about weak lensing, parameters constraints, and Fortran 90 *computation; Charlotte Zanidakis, Academic Programs Administrator, for her kindness and her help when I arrived; Pr. Steven Balbus (ENS, Paris) for advising me when I was looking for this internship; and finally all the people I met here who made this internship a very pleasant experience.*

Contents

Introduction

Modern cosmology began in 1929, with Hubble's discovery that galaxies were receeding from us with a velocity proportional to their distance, the constant of proportionality being the infamous Hubble constant[1]. This observation implies that our Universe is *dynamic*. This overturned Einstein's belief in a static universe, a belief so strong that he had modified general relativity by adding a "cosmological constant". It eventually gave rise to a whole new vision of our cosmic history and fate, bringing deep and almost metaphysical interrogations: why is it expanding? If it is expanding, what happens if we go back in time? Is there a "begining"? Then, will it expand forever? These questions would eventually lead to outstanding theories and improvements of our knowledge of the Universe.

Based on General Relativity (Einstein, 1916), and assuming as its first principle the homogeneity and isotropy of the universe on large (properly cosmological) scales, the theory predicts different histories for our universe. These different cosmological models depend on only a few parameters: the energy density of the components of the Universe, the curvature of the Universe and the Hubble constant. These parameters only depend on the large scale properties of the Universe. The confrontation between general relativity and the observational data has led to the introduction of weakly interacting, invisible, "dark" matter[2], which seems to be the major component of matter in the universe. It also led to the reintroduction of the cosmological constant as a "dark energy" term[3, 4], with negative pressure, which makes the expansion accelerate. This mysterious dark energy has recently been generalized to Quintessence[5], a smooth, space-time varying scalar component with an equation of state $w = P/\rho$, where P is the pressure and ρ the density. The value $w = -1$ corresponds to the usual cosmological constant model. Constraining this w is one of the new goals of modern cosmology.

What is the dark matter? What is the dark energy? By making more detailed measurements, cosmologists are able to constrain the parameters describing these quantities. The *Cosmic Microwave Background* (CMB) gives them the best opportunity to do so. Discovered in 1965 by A.Penzias and R.Wilson of Bell Labs[6], this isotropic and almost homogeneous microwave signal comes from the early universe. It has a spectrum of a perfect black body, and it gives us, through its small fluctuations in temperature of order $\Delta T/T = 10^{-5}$, precious information on the cosmological parameters. The physics of the CMB was soon understood, and the distribution of temperature fluctuations at different scales modeled. The first CMB data was provided by the Cosmic Background Explorer satellite (COBE), a satellite launched in 1989, but were too noisy to allow real precision cosmology to be done. In 2001, the Wilkinson Microwave Anisotropy Probe (WMAP) satellite was launched. Its higher resolution enabled to probe the CMB and constrain parameters at higher precision.[7] The part of data analysis work concerning the cosmological parameters constraint has been done by the team of David Spergel, chairman of the Department of Astrophysical sciences of Princeton University, with whom I worked on the present project. Next year, a new satellite called PLANCK will be launched by the European Space Agency (ESA). Its higher resolution should allow to probe very small scales in the CMB. These are the scales of interest for our work.

While previous studies have focused on using *primary anisotropies* due to fluctuations in the early universe to constrain cosmological parameters, I will focus on using *secondary fluctuations* to constrain dark energy properties. Indeed, as the microwave background photons propagate from the early universe to our telescope, they are affected by metric fluctuations. One of the important alterations is due to the

lensing CMB photons experience when they travel nearby massive objects, such as galaxies or galaxy clusters. In fact, this *weak lensing* is mostly due to the dark matter surrounding these massive objects we see. Thus the knowledge of this effect can inform us of the dark matter distribution in the universe *via* the measure of the so-called *convergence*, an estimator of how lensed the CMB is on different scales. Cross-correlating our convergence maps with the galaxy distribution observed through a galaxy survey can therefore be another way of extracting information from the CMB. Indeed, we should be able to constrain how well visible matter traces dark matter — information encapsuled in a *bias parameter* b, which is just the ratio between visible mass fluctuations and dark matter fluctuations —, as well as how strong these fluctuations are — giving us information on the dark energy w parameter, which determines the acceleration of expansion and thus the suppression of the growth of structure. The limitation on the information we can get will irremediably be the noise we have on each measure. Given a fiducial model and noise expectations, one can therefore *forecast* how much information we could get by cross-correlating different signals and how well we could constrain parameters. In our case, we cross-correlate the visible matter density, modeled such as expected to be seen by an upcoming galaxy survey called ADEPT (Advanced Dark Energy Physics Telescope), and the CMB convergence, estimated through a model of the lensed CMB we should observe with the next generation CMB satellite called PLANCK. My work was thus to write codes to get in the first place the basic functions needed for a cosmology related work, then the expected cross- and autocorrelation terms to be able to study the kind of constraints they would lead to. This report focuses on the combination ADEPT+PLANCK, but the code is more general and can be applied to any survey.

The report is structured as follows: the first part gives an introduction to CMB cosmology and fluctuations analysis. The second part presents the model, the cross-correlation methodology and my calculation of a signal-to-noise ratio for the considered cross-correlation. This number tells us if the signal we expect, here the cross-correlation, is high enough compared to the "noise" coming from the different sources. A high Signal-to-Noise Ratio (SNR) is a good indicator of whether the cross-correlation is worth being studied or not. It is a purely theoretical expectation, and it allows us to compare the improvement a survey such as ADEPT could bring compared to actual ones. Following previous work[8], I also implemented a filter improving this ratio by enhancing the high signal regions and suppressing the high noise ones. The last part presents the results of my joint constraint between the galaxy bias parameter b_g, and the Quintessence parameter w, first taken as constant with respect to time. Lastly, we will consider the celestine Quintessence model[9], in which w varies with time, and will try to forecast constraints on the parameters describing this time evolution. The final section outlines future work.

Several appendices can be found in the end of this report. They treat the mathematical developments of our calculations, and provide details on the CMB physics. They are not essential to understanding this report. We also built a notational glossary.

All the codes were written using Fortran 90, and plots were produced with SM.

I A basic CMB toolkit

We first give the basic tools to understand the physics of the CMB. We need for this purpose to introduce basic concepts of cosmology (in what approximations we work, what notations we use...), as well as the tools for the fluctuations analysis.

I.1 An introduction to cosmology

I.1.1 The expanding universe

In 1929, Edwin Hubble released a paper[1] that would deeply change our understanding of our universe as we experience it. Studying the spectral shift of nearby galaxies, he found a simple relationship between their distance from us and their radial velocity, now known as the *Hubble's law*:

$$v = H_0\, r \tag{1}$$

where H_0 is *Hubble's constant*, traditionnaly measured in kilometers per second per megaparsec[1]. This expansion is universal and has no center. The explanation of this effect is that space itself is expanding as time progresses. This time dependence can be expressed by the dimensionless *scale factor* $a(t)$, with a conventional value $a_0 = 1$ at present. If two objects do not have any peculiar velocity relative to each other, their recession due to the expansion of the Universe would only be due to this factor and their distance would be:

$$r(t) = a(t)\,\eta \tag{2}$$

where η is the *comoving distance*, which doen't depend upon the evolution of the Universe. If the objects have a peculiar velocity relative to each other, this comoving distance would depend upon time. This allows us to define the *comoving coordinates*: if we think of a grid filling the Universe, the physical distance between two nodes would increase with time as the Universe expands, but the comoving distance would keep a constant value as nodes have no peculiar velocity relative to each other.

Since $v = \dot{r}$, where the dot stands for a derivative with respect to time d/dt, we get that

$$\boxed{H(t) = \frac{\dot{a}}{a}} \tag{3}$$

We can see in this form that the Hubble constant $H(t)$ parametrizes the rate of expansion at time t, with a present rate $H_0 = \dot{a_0} \simeq 70$ km.s^{-1}.Mpc^{-1} $\simeq 7 \times 10^{-2}$ Gyr^{-1}. That's the reason why $H(t)$ is usually referred to as the *Hubble rate*. Its inverse gives the characteristic time scale over which the universe expands appreciably. In the following, we will also use the dimensionless parameter h, traditionnaly defined as

$$h = \frac{H_0}{100 \text{ km.s}^{-1}.\text{Mpc}^{-1}} \tag{4}$$

I.1.2 Time variables

Conformal time

In the last paragraph, I used the conventional notation of denoting quantites at present time by the subscript "$_0$". Hence, t_0 is the age of the universe: $t_0 \simeq 13.7$ Gyr. We also use the common practice of setting the speed of light c equal to one. Making the speed of light dimensionless forces us to measure time in units of distance, as it is usually done with the familiar "light year". Considering the distances and times at stake, the natural unit is the megaparsec (Mpc). It is also of use to express distances in terms of h^{-1} Mpc, convention that we used in our codes.

[1] 1 Mpc = $3.08568025\,10^{22}$ m

Let us now introduce the conformal time. In system of unit, light travels during a small amount of time dt the physical distance $dr = dt$. Making use of equation (2), we see that light travels a *comoving* distance $dt/a(t)$. Integrating this quantity since the beginning of the Universe yields the *conformal time* τ, defined as :

$$\boxed{\tau(t) = \int_0^t \frac{dt'}{a(t')}} \tag{5}$$

The conformal time is a useful variable and has a clear physical interpretation. Indeed, at conformal time τ, the maximum comoving distance light could have traveled since the Big Bang is τ itself. We can therefore think of τ as the *comoving horizon*: objects separated by a greater comoving distance than the comoving horizon could never have exchanged information, and thus are *not* in causal contact, whereas objects separated by a shorter distance than τ are said to be in in causal contact. The comoving horizon today is τ_0, the conformal time since the Big Bang, and its value depends on the history of the universe, that is to say on the *cosmology* of the universe.

For questions of simplicity, we will use in the rest of the discussion the *lookback conformal time*. It is the same as the comoving distance for $c = 1$, and is defined as:

$$\boxed{\eta = \tau_0 - \tau} \tag{6}$$

Redshift

Another measure of "distance", or equivalently of "time", is given by the *redshift* z to a particular epoch. Its use is very common in observational astronomy, for it is a feature in the stellar objects electromagnetic spectra which is easily measurable: the redshift is the amount by which an object's spectrum is Doppler shifted due to its velocity relative to the observer. If an object emits radiation at wavelength λ_e, but we observe it at wavelength λ_0, the redshift is given by:

$$z = \frac{\lambda_0 - \lambda_e}{\lambda_e} \tag{7}$$

Thus, objects that are stationary with respect to the observer have redshift zero. However, if two objects are stationary relative to each other in comoving coordinates, they will experience a Doppler shift due to the expansion of the Universe. This specific redshift, which is different from any other kind of redshift (non relativistic and relativistic Doppler redshifts due to peculiar motion in comoving coordinates, gravitational redshift due to the the distortion of space-time), is called the *cosmological redshift*. Its relationship with the scale factor, a complete calculation of which is given in appendix A, is quite simple:

$$\boxed{a(t) = \frac{1}{1 + z(t)}} \tag{8}$$

Thus the higher the redshift is, the smaller the scale factor and thus physical distances are, leading to a singularity at infinite redshift: the Big Bang.

I.1.3 Energy densities

Now that we have defined our time variables, we can describe the dynamics of our Universe. For a homogeneous and isotropic Universe, Einstein equations relating the metric to the energy density reduces to the Friedmann equations. They constitute the basic set of equations needed to describe a Universe's cosmology. We will not enter the details, which are treated in appendix B, and will just give the main and most useful equations for our purpose :

$$\boxed{H(a) = \frac{\dot{a}}{a} = H_0 \sqrt{\frac{\Omega_{r,0}}{a^4} + \frac{\Omega_{m,0}}{a^3} + \frac{\Omega_{k,0}}{a^2} + \Omega_\Lambda}} \tag{9}$$

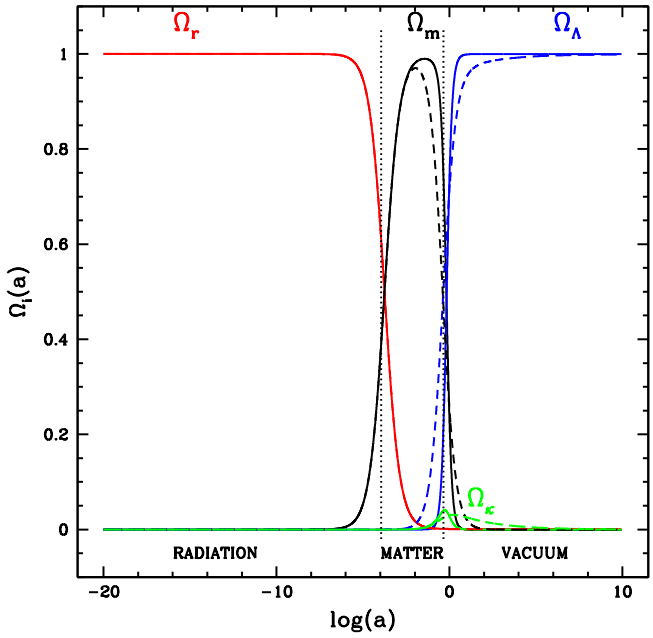

FIG. 1: Relative energy densities $\Omega_i(a)$ versus scale factor. I took the present values to be $\Omega_{m,0} = 0.27$, $\Omega_{r,0} = 5 \times 10^{-5}$, $\Omega_\Lambda = 0.7$, $\Omega_{k,0} = 1 - \Omega_{m,0} - \Omega_{r,0} - \Omega_\Lambda$. Solid lines are for a cosmological constant model, and dashed lines are for a quintessence model with $w = -0.4$. Dotted lines delimit 3 different domination epochs: radiation, matter, and vacuum energy. Vacuum energy dominates earlier for a quintessence model. The curvature energy density and w parameter are exagerated for the purpose of the example, in fact $\Omega_{k,0} \sim 0$ and $w < -0.7$.

Let us explain the meaning of this equation. The total energy in the Universe is considered split into 4 different components. The first one accounts for radiation, relativistic matter (accounting for usual *and* dark matter, called Hot Dark Matter or HDM): these are the photons, neutrinos and exotic relativistic particles. The second one accounts for non relativistic matter (the dark matter part being referred to as Cold Dark Matter or CDM). The third one is the global curvature of the universe (closed, flat, or open), and the last one is the cosmological constant. One can define the energy density of each component i ($i = r$ for radiation, m for matter, k for curvature, Λ for the cosmological constant) at time $\eta(a)$ by

$$\frac{\Omega_i(a)}{\Omega_{i,0}} = \frac{{H_0}^2}{H(a)^2 a^{3\,(1+w_i)}} \tag{10}$$

where $\Omega_{i,0}$ is its present value[2], and $w_i = P_i/\rho_i$ is the ratio between pressure and density for a given component, with $w_i = 1/3$ for radiation, 0 for matter, $-1/3$ for curvature, and -1 for a cosmological constant. Quintessence generalizes the latter by just assuming a fluid with negative pressure: $w_\Lambda < 0$. Except in **III**, we will take $w_\Lambda = w = -1$. These densities give us the normalized repartition of the total energy in the universe among its different components : $\Omega_r(a) + \Omega_m(a) + \Omega_k(a) + \Omega_\Lambda = 1$. This is equivalent to eq.(9).

The interesting feature of this equation is that as $a \to 0$ (i.e as we go back in time), different terms dominate, depending on their w_i (fig.1). We live today in the cosmological constant domination epoch. The cosmology which includes the cosmological constant and cold dark matter is referred as ΛCDM.

[2]Note that it is of use to introduce the quantites $\Omega_{i,0}h^2$, sometimes referred as the "physical parameters", that appear naturally in the equation.

An interesting calculation is given by deriving eq.(9) with respect to time. In the case of a flat universe dominated by cold dark matter and a cosmological constant, we find the acceleration rate of the scale factor :

$$\frac{\ddot{a}}{a} = {H_0}^2(\Omega_\Lambda - \frac{\Omega_{m,0}}{2a^3}) \tag{11}$$

In a flat universe with a cosmological constant, expansion is due to accelerate eventually. This seems to be the case in our universe, and we calculate a present value $\ddot{a}_0 \simeq 3 \times 10^{-3}$ Gyr^{-2}.

Once we have defined our cosmology, we can easily get the value of the lookback conformal time η at redshift z. We first notice that

$$\frac{dt}{a} = \frac{da}{\dot{a}\,a} = \frac{da}{H(a)a^2} = -\frac{dz}{H(z)} \tag{12}$$

Then, given that $\eta(t) = \int_t^{\tau_0} \frac{dt}{a}$, we get the final result:

$$\boxed{\eta(z) = \int_0^z \frac{dz'}{H_0\sqrt{\Omega_{r,0}(1+z')^4 + \Omega_{m,0}(1+z')^3 + \Omega_{k,0}(1+z')^2 + \Omega_\Lambda}}} \tag{13}$$

For very low redshifts, we simply get $\eta(z) = z/H_0$, but for redshifts higher than 0.1, the relation is non linear (an example will be given later in fig 6). For information, the farthest observed stellar objects in the universe (the quasars) are at redshift $z \sim 6$.

I.1.4 The Cosmic Microwave Background

Because of the expansion of the Universe, radiation waves are being "stretched", resulting in a global diminution of temperature as expansion progresses, that is to say for decreasing redshifts (see appendix B, eq.(B.3)). Thus if we go back in time, temperature increases to reach an infinite value at Big Bang, so that there must be a time before which the Universe was entirely ionized. The transition the Universe experienced when temperature was low enough to allow electrons to bind with protons is called *recombination*[3]. At the same time, photons, which were strongly coupled to the primordial plasma through Thomson scattering off free electrons, see their mean free path increase dramatically as they interact very few with the newly formed atoms: this is *decoupling*[4]. These are the photons we see today in the *Cosmic Microwave Background* (CMB), and the surface in the celestial sphere they are coming from is called the *Last Scattering Surface*. The CMB has the spectrum of a nearly perfect black body with observed temperature $T_{\rm CMB} = 2.725 \pm 0.002$ K.[10] The fact that it is the best observed black body in nature shows how strong the coupling between photons and baryons in the primordial plasma was and how opaque the primordial Universe must have been. Considering that decoupling happened at $\sim 3\,000$ K, we deduce the redshift at recombination: $\boxed{z_{\rm rec} \sim 1100}$. At this redshift, the Universe was only 300 000 years old, compared to its 13.7 Gyr today. The CMB is isotropic and nearly perfectly homogeneous, the fluctuations in temperature being of order $\Delta T/T = 10^{-5}$. This is the most encouraging verification of the cosmological principle. We can see on fig.2 that fluctuations in temperature are randomly distributed on the sky. However, their statistical study on different scales is well known, as is the way lensing modifies this distribution.

[3] This is a *re*-combination, even if there was no previous combination of protons and electrons.

[4] We make here the so-called *approximation of strong coupling*, where recombination and decoupling happened at the same time

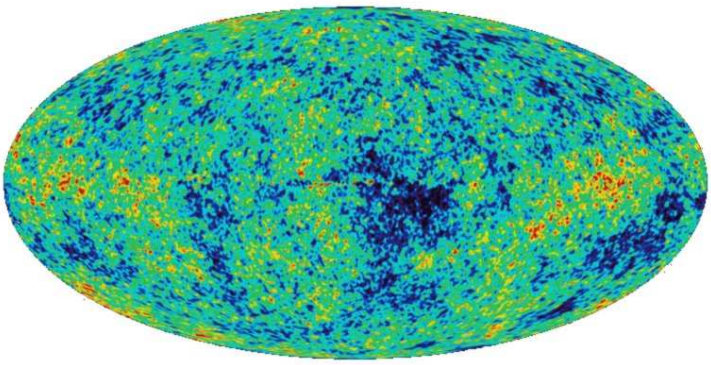

FIG. 2: A projected map of the CMB temperature fluctuations on the celestial sphere, as measured by the WMAP experiment.[11] Colors from blue to red indicate "colder" to "hotter" spots, the strength of these fluctuations in temperature being of order $\Delta T \sim 10\ \mu$K .

I.2 The fluctuations analysis

CMB fluctuations

Since we just use the CMB as a background on which lensing acts by distorting fluctuations, we do not discuss the details of their origin here, but defer the discussion to appendix C. They are the result of density fluctuations in the primordial photon-baryon plasma. These fluctuations are oscillating because of the photon pressure acting against the gravitational pull. Their scale is set by the sound horizon at that time. The strength of these fluctuations and their scale depend on our cosmological parameters. Because we want to characterize fluctuations on the sky (which is a two sphere), the standard convention is to use the spherical harmonic decomposition, equivalent of a Fourier decomposition on a sphere. Denoting by $\Delta T(\hat{n}) = T(\hat{n}) - \langle T \rangle$ the fluctuation in temperature at a position $\hat{n}$ in the sky, with $\langle T \rangle = T_{\rm CMB}$, one can define the fluctuations spherical harmonics decomposition by:

$$\frac{\Delta T(\hat{n})}{\langle T \rangle} = \sum_{\ell=0}^{\infty} \sum_{m=-\ell}^{\ell} a_{\ell m} Y_{\ell m}(\hat{n}) \tag{14}$$

where $Y_{\ell m}(\hat{n})$ is the spherical harmonic of multipole moment ℓ and order m. All the information is contained in the coefficients $a_{\ell m}$, which determine the strength of CMB oscillations at angular scale $\theta \sim 180/\ell$ degrees. As the distribution of the $a_{\ell m}$'s is Gaussian[5], all the information is in fact in the temperature angular power spectrum, which gives the strength of the fluctuations at scale θ. For Gaussian random-phase fluctuations, it is given by :

$$\langle a_{\ell m} a^*_{\ell' m'} \rangle = \delta_{\ell \ell'} \delta_{m m'} C_\ell^{TT} = \frac{1}{2\ell + 1} \sum_{m=-\ell}^{\ell} |a_{\ell m}|^2 \tag{15}$$

Moreover, when we get the data from a CMB observation, we also have a noise on each C_ℓ^{TT} we calculate. This noise ΔC_ℓ^{TT}, which is like a second variance, or *covariance*, has two different origins. The first one is purely statistical: for a given multipole ℓ we only have $(2\ell + 1)/2$ different independent $a_{\ell m}$'s to average over[6]. We thus have an intrinsic noise, named *cosmic variance*, which is simply a Poisson noise $\propto [(2\ell + 1)/2]^{-1/2}$. Moreover, if there is only a fraction $f_{\rm sky}$ of sky covered by the observation, we proportionnaly decrease the information, and finally:

[5] This assertion has been upheld by observational evidence.[12]

[6] The negative m's give the same contribution than the positive ones for a given ℓ.

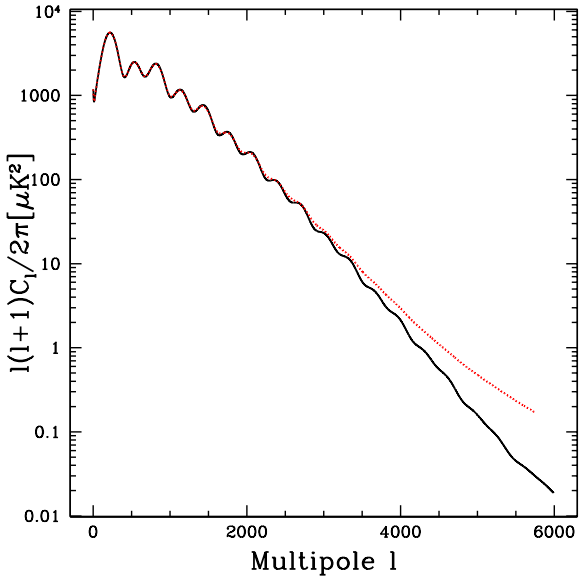

FIG. 3: Temperature angular power spectrum from WMAP for a flat universe with ΛCDM cosmology $\Omega_{m,0} = 0.266$, $\Omega_{\Lambda,0} = 1 - \Omega_{m,0}$, and $H_0 = 70.9$. Compared to our definition, it is multiplied by $T^2_{\rm CMB}$ and given in μK^2. The red dotted line is obtained by taking into account lensing by foreground matter. We adopt an unusual convention here ($\log C_\ell$ - linear ℓ instead of log - log) to emphasize the effect, important on small scales.

$$\left(\Delta C_\ell^{TT}\right)_{\text{cosmic variance}} = \sqrt{\frac{2}{(2\ell+1)f_{\rm sky}}}\, C_\ell^{TT} \tag{16}$$

Then, the signal C_ℓ^{TT} itself has a systematic noise due to the instrumental properties. The CMB maps we get have a certain pixelization that is usually set to be about half the beam width. Considering the beam as gaussian, it is of use to take its angular size to be the Full Width at Half Maximum[7] (FWHM) σ_b, yielding a solid angle $\Delta\Omega = {\sigma_b}^2$. Considering that the errors in the temperature measurement of each pixel are uncorrelated and have a variance ${\sigma_n}^2$, the total variance is then given by $w^{-1} = \Delta\Omega\, {\sigma_n}^2$ (equivalent to divide the noise per pixel by the total number of pixels). Moreover, the finite beam width acts like a "cut-off" for signal on scales smaller than σ_b by convolving the map with a function of the beam shape and size, a Gaussian function in our case. The total detector noise is finally given by[13]:

$$C_\ell^{\rm noise} = w^{-1} e^{\ell^2 {\sigma_b}^2/(8\ln 2)} \tag{17}$$

Adding this noise contribution to the signal in eq.(16), we get the CMB covariance:

$$\boxed{\Delta C_\ell^{TT} = \sqrt{\frac{2}{(2\ell+1)f_{\rm sky}}}\left(C_\ell^{TT} + C_\ell^{\rm noise}\right)} \tag{18}$$

This equation can in fact be generalized to the variances of all the C_ℓ's we will study.

We show on fig.3 the variations of the angular power spectrum with multipole, higher multipoles being smaller scales. The convention is to write $\langle T\rangle^2 \ell(\ell+1)C_\ell^{TT}/2\pi$ in units of μK^2 versus ℓ. We also show the effect of lensing by the foreground matter distribution. It is important on small scales. To quantify this effect, it is of use to introduce the *deflection angle* $\hat{d}$: this is the oriented angle by which a photon trajectory is modified due to lensing, and thus by which the image we see is moved away from the original image. In other words, a fluctuation at $\hat{n}$ will be seen at $\hat{n}+\hat{d}$ by the observer : $\Delta T_{\rm unlensed}(\hat{n}) = \Delta T_{\rm lensed}(\hat{n}+\hat{d})$. We

[7] It is related to the Gaussian variance through $\sigma_{\rm FWHM} = 2\sqrt{2\ln 2}\,\sigma_{\rm Gaussian}$

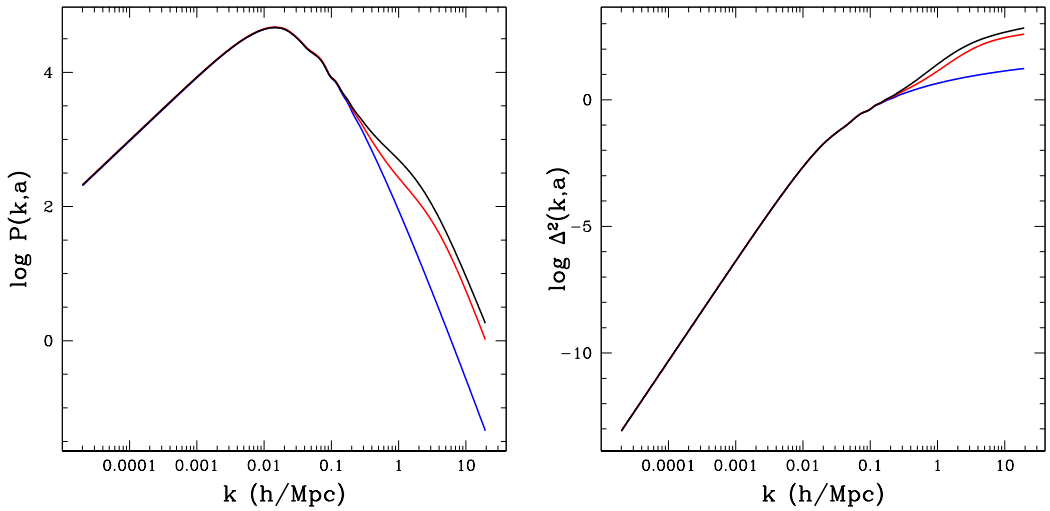

FIG. 4: Matter power spectrum (left) and matter density variance (right). Blue curves are for $a = 0.1$, red curves for $a = 0.5$ and black curves for $a = 1$ (today). We can see for $\Delta(k, a)^2 > 1$ the non linearities grow with time. We have divided each curve by the corresponding growth factor so that the amplitudes are the same.

then can understand quantitatively how the fine-scale anisotropies in the CMB temperature field can trace lensing structures on much larger scales: the rms deflection angle of a CMB photon by foreground structure is only $\langle|\hat{d}_{\rm CMB}|^2\rangle^{1/2} = 2'.6$ in a ΛCDM model, whereas its coherence scale (the scale under which photons experience approximately the same, coherent deflection), given by the position of the maximum in the deflection variance C_ℓ^{dd}, is of a few degrees ($\ell \sim 40$).[14] This type of lensing that only have an impact on the distribution of background fluctuations by smoothly deflecting light rays through the foreground large scale structure is called *weak lensing*, by opposition to the strong lensing that depends on the geometry of the situation and creates strong effects.

Matter density fluctuations

The CMB observation measures density fluctuation at redshift $z_{\rm rec} \sim 1100$. Since that time, photons have been free to travel and matter has been able to clump due to the absence of photon pressure. Thus, fluctuations have been growing, finally giving the structure we see today: stars, galaxies, clusters... To study these fluctuations, we again use Fourier techniques.

Denoting by $n_g(\vec{x})$ the *comoving* number density of galaxies at $\vec{x}$, we can characterize the inhomogeneities with the quantity $\delta_g(\vec{x}) = \frac{n_g(\vec{x}) - \langle n_g\rangle}{\langle n_g\rangle}$. Using for its Fourier transform the same notation, we define the *matter power spectrum* $P(k)$ via:

$$\langle \delta_g(\vec{k}) \delta_g^*(\vec{k'})\rangle = b_g^2\, P(k) \delta_D^3(\vec{k} - \vec{k'}) \tag{19}$$

Here the average brackets denote an average over the whole distribution of galaxies, and δ_D is the Dirac delta function. We have introduced the galaxies *bias parameter* b_g. Its introduction results from the assumption that visible matter fluctuations (obtained here through a galaxy survey) are biased linearly with respect to dark matter fluctuations, which give the "true" matter power spectrum: $\delta_g(\vec{x}) = b_g\, \delta(\vec{x})$, where $\delta(\vec{x})$ is the dark matter fluctuation at comoving position $\vec{x}$. For simplicity, the bias parameter is assumed constant and independent of scale and redshift.

The power spectrum has units of (length)^3. It is sometimes expressed as a dimensionless function by multiplying $P(k)$ by k^3, defining the density variance $\Delta^2(k) \equiv \frac{k^3 P(k)}{2\pi^2}$. We simply have $\Delta < 1$ for small homogeneities and $\Delta > 1$ for large ones. A typical measure of these inhomogeneities is given by σ_8, the

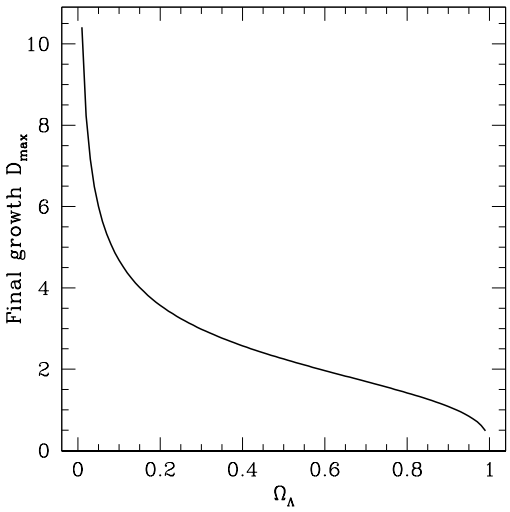

FIG. 5: Evolution of the maximum growth of structure $D_{\max}$ as a function of Ω_Λ in the case of a flat ΛCDM cosmology $\Omega_{m,0}+\Omega_\Lambda = 1$. For increasing cosmological constant, growth is more and more suppressed, as structures stop forming earlier.

mean density variance in spheres of radius 8 h^{-1}Mpc. Its value indicates the "strength" of inhomogeneities at our present time.

What we just defined is the primordial, non evolved, linear power spectrum. Similarly as the temperature angular power spectrum, it peaks at the scale of the comoving sound horizon at matter-radiation equality. We can see wiggles as well. These oscillations in the matter power spectrum are refered to as *Baryon Acoustic Oscillations* (BAO), and are an imprint of the oscillations in the primordial plasma. Smaller scales entered the horizon at earlier times (during radiation domination), and saw their gravitational potential and thus their power decay. Bigger scales entered the horizon later and have a *scale-free* power spectrum $P(k) \propto k^{n_s}$, where $n_s \sim 1$ is the *spectral index*, whose value is a prediction of inflationary models.

Since recombination, this primordial power spectrum has evolved with time as inhomogeneities grew: its amplitude has increased and it has become non linear on small scales ($\Delta^2(k) > 1$). The evolution of amplitude can easlily be quantified by the *linear growth factor* $D(\Omega_{m,0}, a)$, describing the linear growth of inhomogeneities, defined such that $\delta(\vec{x}, a)/D(\Omega_{m,0}, a)$ is constant with time (or with scale factor a), with $\delta(\vec{x}, a)$ the comoving matter density fluctuation at comoving position $\vec{x}$ and conformal lookback time η corresponding to the scale factor $a(\eta)$. Its value is given by the relationship[15]

$$D(a) = \frac{5\Omega_{m,0}}{2}\frac{H(a)}{H_0}\int_0^a da' \left(\frac{H_0}{a'H(a')}\right)^3 \tag{20}$$

During matter domination, this simply reduces to a. But when vacuum energy starts dominating for $a > a_{eq} = (\Omega_{m,0}/\Omega_\Lambda)^{1/3}$ (obtained through $\Omega_{m,0}/a^3 = \Omega_\Lambda = 1 - \Omega_{m,0}$), growth is suppressed and tends eventually to the constant value $D_{\max} = 9\,a_{\rm eq}/4$. We see on fig.5 the importance of this suppression for a given cosmological constant.

The non linearities, on the other hand, can only be approximated by numerical methods. We show in fig.4 the linear and non linear power spectrum and density variance at different times. We divided by the growth factor to keep a constant normalization.

II Signal-to-noise calculation

The following section presents the model we used for our work, the cross-correlation formalism and the signal-to-noise calculation.

II.1 The model

II.1.1 Our cosmology

We base our calculations on a ΛCDM cosmology with flat Universe ($\Omega_{k,0} = 0$) and no radiation[8], so that $\Omega_{m,0} + \Omega_\Lambda = 1$. Given that we study matter clustering correlated with CMB lensing, we take as our fiducial cosmological values the best fit parameters given by the WMAP three-year results along with BAO measurements[16]:

$$\boxed{\begin{aligned} H_0 &= 70.9 \text{ km.s}^{-1}\text{.Mpc}^{-1} \\ \Omega_{m,0} &= 0.266 \\ \Omega_{b,0} &= 0.0446 \\ \Omega_\Lambda &= 0.734 \\ n_s &= 0.951 \\ \sigma_8 &= 0.78 \end{aligned}} \tag{21}$$

where H_0 is the Hubble constant, $\Omega_{m,0}$ the total matter density including dark matter, $\Omega_{b,0}$ the baryonic density (only "usual" matter), Ω_Λ the cosmological constant, n_s the spectral index and σ_8 the mean density variance in spheres of radius $8\,h^{-1}$Mpc. These quantities are given at present time, and have been defined in **I.1.3**.

Inserting these values in eq.(13), we find a comoving distance to the Big Bang $\eta_0 = 14\,672$ Mpc and a distance to recombination $\eta_{\text{rec}} = 14\,178$ Mpc. We show on fig.6 the comoving distance versus redshift for our cosmological model.

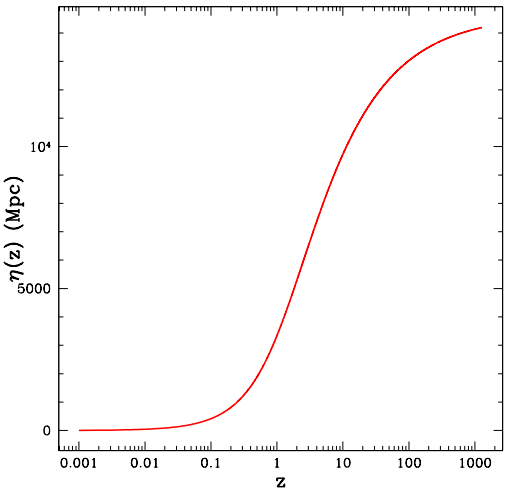

FIG. 6: Lookback conformal time $\eta(z)$ versus redshift, with our cosmological parameters $\Omega_{m,0} = 0.266$, $\Omega_{\Lambda,0} = 1 - \Omega_{m,0}$, no curvature nor radiation, and $H_0 = 70.9$ km.s^{-1}.Mpc^{-1}.

[8] The approximation of no radiation is justified by the fact we work until $a \simeq 10^{-3}$, when radiation already ceased to dominate (fig.1).

II.1.2 Expected observational properties

- *ADEPT*

To describe a redshift survey, we have to specify certain parameters: the range of redshifts studied, the number of objects expected to be seen considering the flux limit, and the sky coverage. In the case of ADEPT, we expect to see 100 million galaxies uniformly distributed between redshifts 1 and 2 on a sky area of $28,600$ deg^2. To take into account the sky coverage, we define the fraction of sky covered f_{sky} as the ratio between the sky surface covered and the total sky surface of $4\pi(\frac{180}{\pi})^2\,\text{deg}^2 \sim 41,000\,\text{deg}^2$. For PLANCK, we have[9] $f_{\text{sky}} = 0.8$, and for ADEPT $\boxed{f_{\text{sky}} = 0.7}$, so we take the latter to be our true fraction of sky covered for the cross-correlation. Because of the flux limit and the range of redshifts in which we observe, we only see a certain distribution of galaxies. This can be encompassed in a normalized redshift distribution function $W_z(z)$, truly the probability per redshift bin dz to observe a galaxy around z for a given survey. In our case we expect to see a uniform distribution, so that we just have a step function, naturally normalized to unity because of the redshift range $\Delta z = 1$:

$$\boxed{W_z(z) = \begin{cases} 1 & \text{for } 1 < z < 2 \\ 0 & \text{elsewhere} \end{cases}} \tag{22}$$

However, we must be careful when converting into a distribution with comoving distance η as a parameter. Indeed, $W_\eta(\eta)$ is obtained by:

$$W_\eta(\eta)\,d\eta = W_z(z)\,dz \tag{23}$$

yielding in our case

$$W_\eta(\eta(z)) = W_z(z) H_0 \sqrt{\Omega_{m,0}\,(1+z)^3 + (1-\Omega_{m,0})} \tag{24}$$

A computational difficulty that arose when writing the Fortran code to get this distribution was to invert $\eta(z)$. It is simply done by creating arrays for z and η until $z = z_{\text{rec}}$, locating the desired η and interpolating to find z using preexisiting subroutines (in my case, `locate` and `polint` from Numerical Recipes in Fortran 90). However, we need to define logarithmic arrays by fixing a constant stepsize in log space to have a coherent result: in linear space functions are too steep to allow precise interpolations.

- *PLANCK*

For the 217 Ghz HFI bolometer of PLANCK, the noise parameters are[17]:

$$\boxed{\begin{aligned} \sigma_n &= 4.8 \times 10^{-6} \\ \sigma_b &= 5' \end{aligned}} \tag{25}$$

For comparison, WMAP offered the same order of noise per pixel but a FWHM angle 3 times larger ($\sigma_b \sim 13'$), cutting off the signal above $\ell \sim 1000$, whereas PLANCK could obtain data up to $\ell \simeq 2000$. COBE had a FWHM angle $\sigma_b \sim 7$ deg. We compare on fig.7 the errors for PLANCK and WMAP.

The power spectrum is computed through an interface called CAMB, which allows us to get a model spectrum for a given set of cosmological parameters to an accuracy better than $\sim 1\%$.[18]

[9] While PLANCK covers the whole sky, galactic foreground obscure approximately 20% of it.

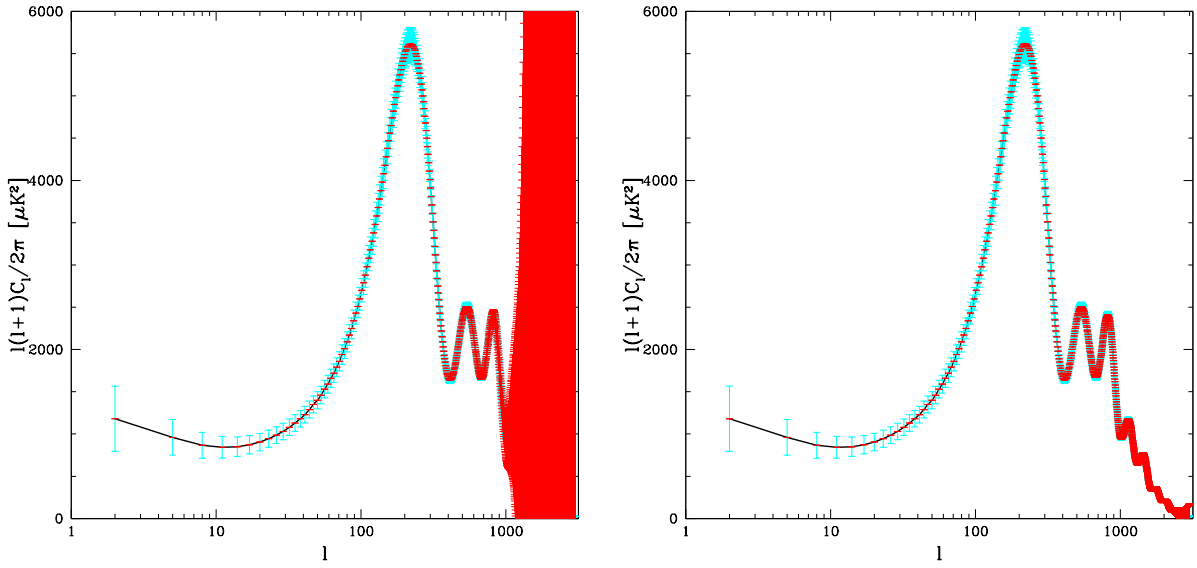

FIG. 7: Temperature angular power spectrum computed with CAMB, with noise from WMAP (left) and PLANCK (right). In blue we show the error due to cosmic variance, in red the detector noise. We have divided our errors by $\Delta\ell^{1/2}$, where $\Delta\ell$ is a bin in multipole (here $\Delta\ell = 3$). For real data points, $\Delta\ell$ is the interval on which we average all the raw data points to one point with error bars.

II.1.3 Quantities of interest for the cross-correlation

In the following, we follow the methodology and notations of previous works[8].

The convergence

Given the low noise attainable with PLANCK, we will have access to more precise information on small scales for the CMB power spectrum, where weak lensing is important. In fact, this lensing is mainly caused by dark matter present between us and the CMB, described by its density fluctuations $\delta(\vec{x}, a)$. Studying the angular power spectrum modification, one can construct an estimator of the *convergence*, quantity characterizing the lensing strength of the foreground matter, as well as an estimator of the noise such a method would generate[14]. Here we introduce the convergence.

The convergence of the CMB in the direction $\hat{n}$ is given by[19]:

$$\kappa_{\rm CMB}(\hat{n}) = \frac{3{H_0}^2\Omega_{m,0}}{2}\int_0^{\eta_{\rm rec}} d\eta\, \frac{\eta\,(\eta_{\rm rec}-\eta)}{\eta_{\rm rec}}\,\frac{\delta(\eta\hat{n},a)}{a(\eta)} \tag{26}$$

where the source is the CMB at $\eta_{\rm rec}$. Basically, we sum over all the lensing material between us and the CMB, each contribution depending on the mass density through $\Omega_{m,0}\,\delta(\eta\hat{n},a)$. Here relies the information on the underlying mass distribution. The geometrical weight $\frac{\eta\,(\eta_{\rm rec}-\eta)}{\eta_{\rm rec}}$ is equivalent to the focal length in geometrical optics: it appears with the condition that the observer sees the deflected light from the source object, and it gives more importance to intermediate distances between us and the CMB. Such distances correspond to a broad redshift range peaked around $z \sim 3$. That is why we think that deep redshift surveys such as ADEPT could get better information from the lensed CMB. The weak lensing limit corresponds to $\kappa \ll 1$.

We can then expand the comoving density fluctuations as:

$$\delta(\eta\hat{n}, a(\eta)) = \int \frac{d^3\vec{k}}{(2\pi)^{3/2}}\delta(\vec{k}, a(\eta))e^{i\vec{k}.\hat{n}\eta} \tag{27}$$

yielding a final convergence

$$\boxed{\kappa_{\rm CMB}(\hat{n}) = \frac{3{H_0}^2\Omega_{m,0}}{2}\int_0^{\eta_{\rm rec}} d\eta \int \frac{d^3\vec{k}}{(2\pi)^{3/2}}\,\frac{\eta\,(\eta_{\rm rec}-\eta)}{\eta_{\rm rec}}\,\frac{\delta(\vec{k},a(\eta))}{a(\eta)}\;e^{i\vec{k}.\hat{n}\eta}} \tag{28}$$

The projected density fluctuations

We have seen that convergence is a tool to extract information about the dark matter present between us and the CMB. Redshift surveys, on the other hand, allow us to extract information about the *visible* matter distribution, in our case the galaxies described by a density fluctuation $\delta_g(\vec{x},a)$ and a distribution $W_{\eta,\rm gal}(\eta)$. We define the convenient *projected surface density* as the projection of the visible density fluctuations along the line-of-sight. It can simply be written as:

$$\begin{aligned}\Sigma_g(\hat{m}) &= \int_0^{\eta_0} d\eta \frac{n_g(\vec{x})-\langle n_g\rangle}{\langle n_g\rangle} \\ &= \int_0^{\eta_0} d\eta\, W_\eta(\eta) b_g \delta(\eta\hat{m},a(\eta))\end{aligned} \tag{29}$$

where $n_g(\vec{x})$ is the *observed* comoving number density of galaxies introduced in **I.2** and $\vec{x}=\eta\hat{m}$ is the position of the fluctuation along the line-of-sight. The interpretation is simple: we project visible comoving density fluctuations along the line-of-sight, with a weight corresponding to the distribution of galaxies we can actually see with our survey. Using eq.(27) and (29), we write the projected density fluctuations in direction $\hat{m}$:

$$\boxed{\Sigma_g(\hat{m}) = \int_0^{\tau_0} d\eta \int \frac{d^3\vec{k}}{(2\pi)^{3/2}} W_\eta(\eta) b_g \delta(\vec{k},a(\eta))\, e^{i\vec{k}.\hat{m}\eta}} \tag{30}$$

In our code, we also included a small perturbation in our distribution, called the magnification effect, discussed in Peiris & Spergel (2001).[8] Its effect is to slightly broaden the distribution because of the lensing by foreground matter that brings some faint galaxies above the magnitude limit of the survey. However it is not of real importance discussing it here, as we just want a qualitative estimate for simple theoretical distributions.

II.2 The cross-correlation

II.2.1 Analytic approach

Using some mathematical formalism (appendix D.**I**), one can derive the cross- and auto-correlation terms for Σ_g and $\kappa_{\rm CMB}$, which can be written as:

$$C_\ell^{X-Y} = \frac{2}{\pi}\int k^2 dk\, w_\ell^X(k) w_\ell^Y(k) \tag{31}$$

where X and Y stand for Σ_g or $\kappa_{\rm CMB}$. The window functions read:

$$\begin{aligned} w_\ell^{\Sigma_g}(k) &= \int_0^{\eta_{\rm rec}} d\eta\, W_\eta(\eta) b_g \sqrt{P(k,a(\eta))}\, j_\ell(k\eta) \\ w_\ell^{\kappa}(k) &= \frac{3{H_0}^2\Omega_{m,0}}{2}\int_0^{\eta_{\rm rec}} d\eta \frac{\eta\,(\eta_{\rm rec}-\eta)}{\eta_{\rm rec}}\,\frac{\sqrt{P(k,a(\eta))}}{a(\eta)}\, j_\ell(k\eta)\end{aligned} \tag{32}$$

which are roughly our previous quantities with $\delta(k,a)\to\sqrt{P(k,a)}$ and $\int dk e^{i\vec{k}.\hat{n}\eta}\to j_\ell(k\eta)$. We also have approximated $\eta_0\sim\eta_{\rm rec}$ in $w_\ell^{\Sigma_g}$, which is a more than good approximation, since in our case the galaxy distribution cuts the integral after $z=2\ll z_{\rm rec}$.

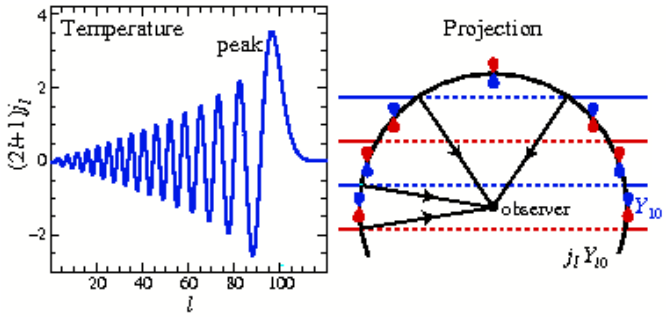

FIG. 8: On the left the Bessel function $j_\ell(100)$ as a function of ℓ and on the right a view of a plane wave fluctuation on the celestial sphere. The Limber approximation replaces the Bessel function by a Dirac delta function where it peaks. This is due to the fact that the observer sees a maximum anisotropy in the sky when looking in a direction parallel to the wave. Figure found in [20].

II.2.2 The Limber approximation

We now introduce the Limber approximation, which we will use in the rest of this report. This approximation consists in converting physical to angular scale: in cosmologist terms, converting flat-sky (plane waves in k-space) to all-sky (spherical harmonics in ℓ-space). We can see on fig.8 that the maximum anisotropy an observer can see on the sky for a plane wave is when he looks in a direction parallel to the waves. The Limber approximation consists in taking the all-sky scale of this flat-sky fluctuation to be the one of the maximum of anisotropy. In the small angle approximation, valid in the large ℓ limit ($\ell \sim \theta^{-1}$) in which we are interested, a fluctuation of comoving wave number k, which scales as k^{-1}, and at conformal distance η will thus verify: $k^{-1} \sim \eta\theta \rightarrow \boxed{\ell \sim k\eta}$. In this approximation, the Bessel function is approximated as[21]:

$$j_\ell(k\eta) = \sqrt{\frac{\pi}{2\ell+1}}\left(\delta_D(\ell+1/2-k\eta) + \mathcal{O}\left(\frac{1}{\ell^2}\right)\right) \tag{33}$$

Since we work in a large ℓ approximation, we will not write the $1/2$ factor in $\ell+1/2$, which will make the calculation clearer. Under this approximation, we get (see appendix **II**):

$$\boxed{\begin{aligned} C_\ell^{\Sigma_g-\kappa} &= \left(\frac{3{H_0}^2\Omega_{m,0}}{2}\right)\int_0^{\eta_{\rm rec}} \frac{d\eta}{\eta}\left[\frac{\eta_{\rm rec}-\eta}{a(\eta)\,\eta_{\rm rec}}\right][b_g W_\eta(\eta)]\,P(\ell/\eta,a) \\ C_\ell^{\Sigma_g-\Sigma_g} &= \int_0^{\eta_{\rm rec}} \frac{d\eta}{\eta^2}\,[b_g W_\eta(\eta)]^2\,P(\ell/\eta,a) \\ C_\ell^{\kappa-\kappa} &= \left(\frac{3{H_0}^2\Omega_{m,0}}{2}\right)^2\int_0^{\eta_{\rm rec}} d\eta\left[\frac{\eta_{\rm rec}-\eta}{a(\eta)\,\eta_{\rm rec}}\right]^2 P(\ell/\eta,a) \end{aligned}} \tag{34}$$

II.2.3 The noise terms

The auto-correlation signals we get exhibit certain noises due to the properties of the experiments.

Convergence noise

To calculate the convergence from a CMB map, we thought we would be using the best estimator proposed by W.Hu in 2001.[14] As we said in **I.2**, the distortion of the small-scale anisotropies in the CMB temperature field traces large scale lensing structures. This lead Hu to use a high-pass filter on the temperature fluctuations to keep the small-scale ones and a low-pass filter on their gradient whose variations scale as the size of foreground matter fluctuations to keep the large scale ones. He derives an estimator of the deflection angle power spectrum and finds the noise for this estimator :

$$(N_\ell{}^{dd})^{-1} = \frac{1}{\ell^2}\int \frac{d^2 l_1}{(2\pi)^2}\frac{(\vec{\ell}.\vec{l_1}\tilde{C}_{l_1}^{TT} + \vec{\ell}.\vec{l_2}\tilde{C}_{l_2}^{TT})^2}{2C_{l_1}^{\rm tot}C_{l_2}^{\rm tot}} \tag{35}$$

where $C_l{}^{TT}$ ($\tilde{C}_l^{TT}$) is the lensed (unlensed) temperature power spectrum, $\vec{\ell} = \vec{l_1}+\vec{l_2}$, and $\tilde{C}_l^{\rm tot} = \tilde{C}_l^{TT}+N_l^{TT}$, with $N_l^{TT} = w^{-1}e^{\ell^2{\sigma_b}^2/(8\ln 2)}$.

By definition, convergence is related to the deflection angle by $\kappa = \frac{1}{2}\vec{\nabla}.\vec{d}$.[22] When working in Fourier space, this writes as $\kappa = -\frac{\vec{\ell}.\vec{d}}{2}$. Therefore, in terms of variance, this yields the convergence noise:

$$\boxed{N_\ell^{\kappa\kappa} = \frac{\ell^2 N_\ell^{dd}}{4}} \tag{36}$$

The computational difficulty is here to compute to the double integrate in N_ℓ^{dd}. I used the routine `rombint`, also used in CAMB, where I can ask for a certain relative precision for the result. I also had to define a cut-off in ℓ_1 for the integration since the estimator is built with the best-fit data available for a given experiment. Considering the case of PLANCK, I took $\ell_{\rm cut} = 2500$ (see fig.7).

Density fluctuations noise

The principal restriction when counting galaxies to evaluate their fluctuations is their finite number. For a fluctuation $\delta_g(\vec{x})$, we thus have a *Poisson noise* of $n_g(\vec{x})^{-1/2}$. Thus, the variance noise we have on $b_g^2 P(k,a)$ is just the square of this, $n_g(\eta)^{-1}$. Using the equation for the auto-correlation in Σ_g (eq.34), we deduce the noise variance:

$$\boxed{N_\ell^{\Sigma_g-\Sigma_g} = \int \frac{d\eta}{\eta^2} W_\eta(\eta)^2 n_g(\eta)^{-1}} \tag{37}$$

Knowing the distribution of galaxies $W_\eta(\eta)$ and the number of galaxies per steradian we see on the sky N_Ω, we deduce how to get the comoving number density:

$$n_g(\eta) = \frac{dN(\eta)}{\eta^2\, d\eta\, d\Omega} = N_\Omega \frac{W_\eta(\eta)}{\eta^2} \tag{38}$$

where $dN(\eta)$ is the number of observed galaxies in the *comoving* volume $\eta^2 d\eta\, d\Omega$. We note that, as expected, the projected Poisson noise goes as N_Ω^{-1}.

II.3 Signal-to-noise for the cross-correlation

II.3.1 A first derivation

The (squared) signal-to-noise per ℓ-mode for our cross-correlation is given by[23]:

$$\left(\frac{S}{N}\right)_\ell^2 = f_{\rm sky}(2\ell+1)\frac{(C_\ell^{\Sigma_g-\kappa})^2}{(C_\ell^{\Sigma_g-\Sigma_g}+N_\ell^{\Sigma_g-\Sigma_g})(C_\ell^{\kappa\kappa}+N_\ell^{\kappa\kappa}) + \underbrace{(C_\ell^{\Sigma_g-\kappa})^2}_{\rm neglected}} \tag{39}$$

The signal-to-noise can be seen as the ratio between the signal we get from the cross-correlation divided by its covariance, which is the sum of a signal term (cosmic variance) and a noise term being the product of the two auto-correlation covariances. This is related to what we said in **I.2** in the case of the CMB : there is a noise due to the experiment itself (beam smoothing, noise per pixel, or Poisson noise in the galaxies case) and a noise proportional to the signal due to the theory of statistics (the cosmic variance term). Since the cross-correlation term is usually very small compared to the auto-correlation terms, it is of use to neglect it in the denominator. We will later see that this estimation is good to ~ 2 % accuracy. The total signal-to-noise is obtained by summing over all the $\ell's$ covered by the experiment.

II.3.2 Filtering technique to maximize the signal-to-noise

Here we adapt previous theoretical work to the case of weak lensing.[8]

What we observe in a redshift survey is the 3D comoving number density. The CMB convergence, however, gives a 2D information. We thus have the freedom to build any 2D map by weighing properly the comoving number density along the line of sight, hoping to increase our cross-correlation signal-to-noise. Our goal is therefore to find the weight function $w_\ell(k,\eta)$ that maximizes it.

The link between the comoving number density n_i and the projected surface density was given in eq.(29). Introducing a weight function in $n_i(\vec{x})$ will thus weight our projected surface density fluctuations along the line-of-sight, changing our cross-correlation and our signal-to-noise. The weighted surface density fluctuations will be written with a tilde: $\tilde{\Sigma}_g$. We can in fact simply add the filter in every necessary place by replacing $W_\eta(\eta)$ by $W_\eta(\eta)w_\ell(k,\eta)$, with $k=\ell/\eta$ in the Limber approximation. The effect of the filter is indeed just to change the observed distribution of objects so that we keep the high signal regions and supress the low signal - high noise ones. The idea is to apply the filter to our correlation terms, and to find the correct filter that will maximize our signal-to-noise by differentiating and putting to 0: $\delta(S/N)/\delta w_\ell = 0$. The whole calculation is presented in appendix E. The convenient, Limber approximated weight is found to be:

$$\boxed{w_\ell(k=\ell/\eta,\eta) = \left(\frac{3{H_0}^2\Omega_{m,0}}{2}\right)\left[\frac{\eta_{\rm rec}-\eta}{a(\eta)\,\eta_{\rm rec}}\right]\frac{\eta}{b_g W_\eta(\eta)}\left(\frac{{b_g}^2 P(\ell/\eta,a)}{{b_g}^2 P(\ell/\eta,a)+\frac{1}{n_g(\eta)}}\right)} \tag{40}$$

We recognize here the projected signal over the projected noise. This weighting seems *a posteriori* quite natural: regions where the noise get large ($n_g(\eta)\to 0$), or equivalently where the signal is weak ($P(k,a)\to 0$), are faded by the filter ($w_\ell \to 0$), while regions of large signal and small noise are enhanced. Introducing this filter in eq.(39) leads to a simplification between one cross-correlation signal $C_\ell^{\Sigma_g-\kappa}$ and the surface density auto-correlation noise $C_\ell^{\Sigma_g-\Sigma_g}+N_\ell^{\Sigma_g-\Sigma_g}$ yielding:

$$\boxed{\left(\frac{S}{N}\right)^2_{\rm filtered} = 2f_{\rm sky}\int \ell d\ell \frac{C_\ell^{\tilde{\Sigma}_g-\kappa}}{C_\ell^{\kappa\kappa}+N_\ell^{\kappa\kappa}}} \tag{41}$$

where we used the Limber small-scales approximation to replace summing by integrating over ℓ and to neglect the 1 in $2\ell+1$. $C_\ell^{\kappa\kappa}$ and $N_\ell^{\kappa\kappa}$ are given in eq.(34) and (36), and

$$C_\ell^{\tilde{\Sigma}_g-\kappa} = \left(\frac{3{H_0}^2\Omega_{m,0}}{2}\right)^2\int_0^{\eta_{\rm rec}} d\eta \left[\frac{\eta_{\rm rec}-\eta}{a(\eta)\,\eta_{\rm rec}}\right]^2 \frac{P(\ell/\eta,a)}{1+\frac{1}{b_g^2 P(\ell/\eta,a) n_g(\eta)}} \tag{42}$$

We show on fig.9 the effect of the filter for our auto and cross-correlations. While our signal, the cross-correlation term $C_\ell^{\Sigma_g-\kappa}$, doesn't change much with the filter, the surface density covariance term, $C_\ell^{\Sigma_g-\Sigma_g}+N_\ell^{\Sigma_g-\Sigma_g}$, is damped. The convergence signal and noise are not affected, as they only depend on the CMB observation.

II.3.3 Results

We wrote a routine for each cross- and auto-correlation term, with the possibility to choose if we apply the filter and if we include non linearities in the power spectrum. The goal in writing routines separately is that it makes it easy to verify if they work correctly. Our code also calculates all the basic functions (the scale factor, the radial galaxy distribution, the comoving number density) for any given set of cosmological parameters and any given b_g. Finally, we can input any properties for the observations (σ_b and σ_n for the CMB, the number of galaxies, sky coverage, and redshift distribution for the galaxy survey), allowing us to compare different models.

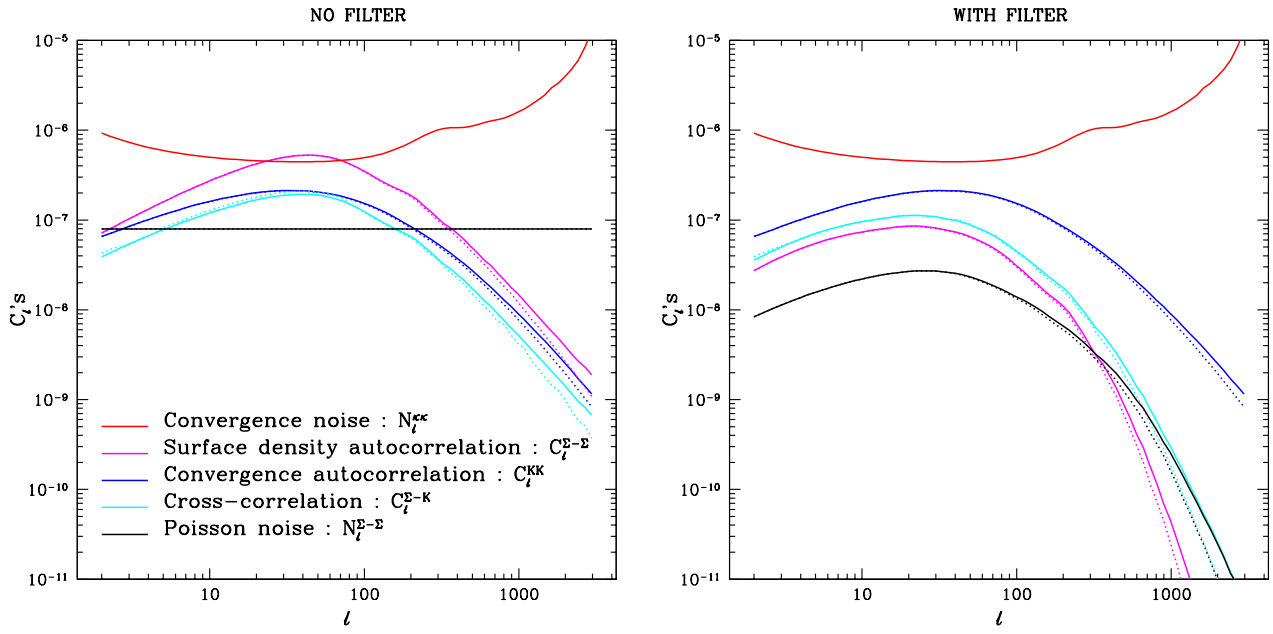

FIG. 9: Our different auto- and cross-correlation terms for a PLANCK+ADEPT combination. On the left, no filter is applied, and on the right we use the optimal filter. In this case, we can see the high signal region ($\ell \sim 40$) is conserved whereas the high noise regions are supressed. Dotted lines are for a linear matter power spectrum, solid lines for a non-linear one: we can see the power raise on small scales where non linearities grow.

Survey	Redshift range	Sky coverage ($\deg^2$)	Number of galaxies ($\times 10^6$)	*Non filtered* S/N	*Filtered* S/N
ADEPT[24]	$1 < z < 2$	28 600	100	50	54
LSST[25]	$0.5 < z < 3.5$	10 000	100	44.8	45.5
Cosmic vision program (ESA)[26]	$1 < z < 2$	28 600	1 000	67	76
SDSS II 8 yrs LRG[27]	$0.16 < z < 0.47$	3800	0.094	5	5
WFMOS / Subaru[28]	$0.5 < z < 1.3$	2 000	2	10	10.5
HETDEX[29]	$1.8 < z < 3.8$	200	1	4.5	5

TAB. 1: Non filtered and filtered S/N for different observations. The first 3 rows are expected observations, the last 3 existing telescopes. We can see that the filter works better for higher S/N.

We take as a reference model the case of the ADEPT survey combined with the PLANCK observation including the filter, with the box distribution presented in **II.1.2** centered around $z_s = 1.5$ and of width $\Delta z = 1$. We take for b_g the value $\boxed{b_g = 1}$, indicating that light traces dark matter quite well.

We show in tab.1 the results for different surveys. We chose the redshift distributions to be normalized box functions inside the specified range of redshifts. The ESA Cosmic Vision Program observation would be similar to ADEPT, except with a higher number of observed galaxies, yielding the highest S/N we could get among all the possible surveys. Because of the $f_{\rm sky}$ factor, the S/N is very sensitive to the sky coverage. Higher galaxies density, *i.e.* high number of galaxies on a given sky patch, will give low Poisson noise and thus high S/N. In our case, we see that we want the observation to be deep in redshift, to

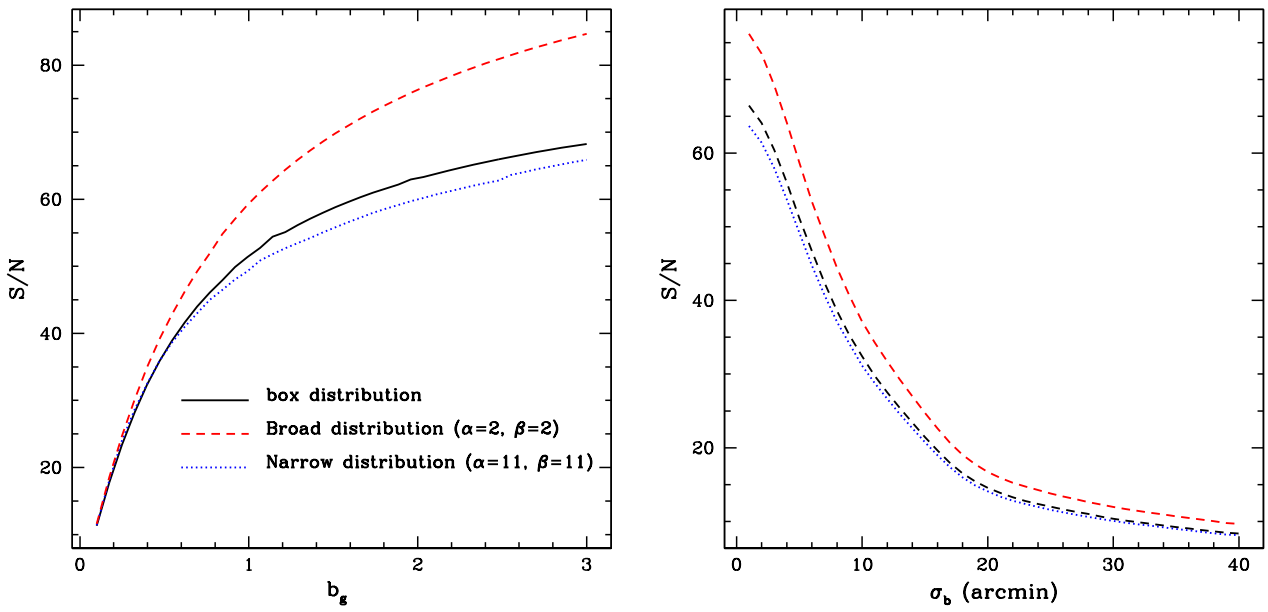

FIG. 10: Variation of the signal-to-noise with the bias parameter b_g (left) and the FWHM beam width σ_b of the CMB survey (right). We compare ADEPT reference box distribution (black solid line) with 2 more realistic distributions, taken to be $W(z) \propto (z/z_s)^\alpha \exp\left[-(z/z_s)^\beta\right]$: a narrow distribution peaked around $z_s = 1.5$ for $\alpha = 11$ and $\beta = 11$ (blue dotted line), and a broad one for $\alpha = 2$ and $\beta = 2$ (red dashed line). All the other parameters are reference parameters. We can see the improvement of the S/N with the bias parameter (more signal) and with better resolution (less noise). Broader distributions improve the statistics as well.

have a large sky coverage, and be sensitive enough to observe as many galaxies as possible. Compared to the expectations one could have had a few years ago (Peiris & Spergel, 2000), which were giving at best $S/N \sim 11$, we can expect dramatic improvements in getting constraints from cross-correlations between the CMB and galaxy surveys with upcoming observations.

We also checked the accuracy of the approximation made in **II.3.1**, where we neglected the signal term in the denominator. The most significant difference we get is for the high S/N of the ESA program, where $S/N \to 74.4$ instead of 76, yielding an error of 2.3 %. Considering the qualitative order of magnitude we are looking for, this is totally acceptable.

In fig.10, we show the variations of the S/N with the bias parameter and with the resolution of the CMB map we observe for different distributions. PLANCK resolution improves the S/N by more than a factor of 2 compared to WMAP. Then, higher bias parameter yields higher S/N: the visible matter distribution we get from galaxy surveys is a better tracer of the dark matter distribution that deflects CMB photons, improving the information we can get from cross-correlating both signals.

Now that we have seen qualitatively that this cross-correlation could allow us to get more information on the parameters and their constraints, we want to quantify it. This is done through a χ^2 study.

III Forecasting the constraint

III.1 χ^2 evaluation

The whole theory of cosmological parameters estimation relies on a probability function called *the likelihood function*[10] $\mathcal{L}(\vec{x},\vec{\alpha})$. This is essentially the probability $P(\vec{x}|\vec{\alpha})$ for a given experiment to get the data $\vec{x}$ given a theory with parameters $\vec{\alpha}$ and a given noise. In our case, $\vec{x}$ is the set of parameters we study (b_g,w) as measured by the experiment (the cross-correlation), and $\vec{\alpha}$ is the set of 'true' parameters that compose our cosmology, which we will note ($\bar{b_g}$,$\bar{w}$). One can invert the probabilites through Bayes' theorem : $P[\vec{\alpha}|\vec{x}]P[\vec{x}] = P[\vec{x}|\vec{\alpha}]P[\vec{\alpha}]$. Assuming weak priors[11] on the parameters $\vec{\alpha}$, one finds that $P[\vec{\alpha},\vec{x}] \propto \mathcal{L}(\vec{x},\vec{\alpha})$: the likelihood function can also be thought of as the probability to have a certain set of parameters given the data we get from the observations. Basically, one draws a curve corresponding to the model for a given set of parameters, compare it to the data points and see if it could be a fit considering the noise of the experiment. Several sets of parameters can thus correspond to what we observe: this is called the *cosmic degeneracy*. How far we can be from the true parameters finally depends on how noisy our experiment is: the less noisy it is, the more discriminatory the experiment is and the more precise our constraint on the parameters can be. Given a *fiducial model* for the parameters, *i.e.* a set of parameters we think describes relatively well what we expect to be the "true parameters", one can forecast how well we could constrain these parameters by studying how fast the likelihood vanishes around this maximum of probability in the parameters space.

Luckily, this forecast can be simply described in our case. Let us first notice that we will not get the parameters directly through the data, but through the cross- and auto-correlations instead. However, as we work around maxima of probability, we suppose our functions expand as simple quadratic functions of the parameters — hypothesis we will indeed be verifying quite well. Then, in the case of Gaussian distributed errors on the estimation, one finds that $\mathcal{L}(\vec{x},\vec{\alpha}) = \mathcal{L}_0 \exp\left(-\chi^2(\vec{x},\vec{\alpha})/2\right)$, where $\mathcal{L}_0$ is a normalization factor and

$$\chi^2(\vec{x},\vec{\alpha}) = \sum_\ell \frac{(C_\ell(\vec{x}) - C_\ell(\vec{\alpha}))^2}{(\Delta C_\ell)^2} \tag{43}$$

where ΔC_ℓ is the covariance of the signal, as introduced in **I.2**. In our case, we must add the contributions from all the correlations, yielding:

$$\chi^2(b_g,w;\bar{b_g},\bar{w}) = 2f_{\text{sky}} \int \ell d\ell \left(\frac{\left[C_\ell^{\tilde{\Sigma}_g-\kappa}(b_g,w) - C_\ell^{\tilde{\Sigma}_g-\kappa}\right]^2}{\left(C_\ell^{\kappa\kappa} + N_\ell^{\kappa\kappa}\right) C_\ell^{\tilde{\Sigma}_g-\kappa}} + \frac{\left[C_\ell^{\Sigma_g-\Sigma_g}(b_g,w) - C_\ell^{\Sigma_g-\Sigma_g}\right]^2}{\left(N_\ell^{\Sigma_g-\Sigma_g}\right)^2} \right) \tag{44}$$

where all the terms without explicit dependence in parameters are taken to be at the fiducial point ($\bar{b_g}$, $\bar{w}$). The first term is recognized as our filtered cross-correlation, with $C_\ell^{\tilde{\Sigma}_g-\kappa} = C_\ell^{\tilde{\Sigma}_g-\tilde{\Sigma}_g} + N_\ell^{\tilde{\Sigma}_g-\tilde{\Sigma}_g}$, and the second term as the surface density auto-correlation. The convergence auto-correlation is neglected since the convergence noise is typically an order of magnitude higher than the signal (see fig.9). Consistent with our signal-to-noise calculation, we neglected the signal terms in the denominators.

Given the χ^2, we can evaluate the error we have on the estimation of the parameters by simply noticing that, since $\mathcal{L} \propto \exp\left(-\chi^2/2\right)$, the values $\chi^2 = 1,2,3...$ give the $1-\sigma$, $2-\sigma$, $3-\sigma$... regions of probability of the likelihood function, that is to say the zones in the parameter space in which we are confident at 68.3%, 95.5% and 99.8% that it contains the true parameters.

[10] One can find a complete review of this theory in the last chapter of *Modern Cosmology*, Dodelson (2003)[15].

[11] If the data have disciminatory power, which is our case, then the likelihood function will be sharply peaked and any reasonable prior will not affect the final results.

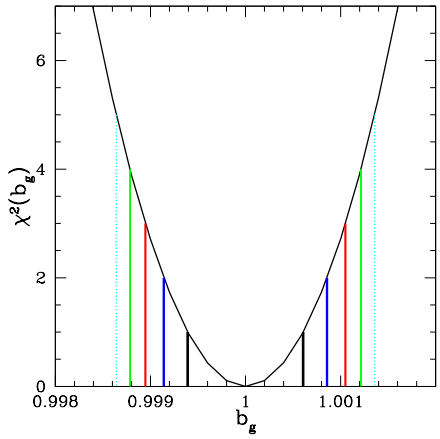

FIG. 11: $\chi^2(b_g)$ for a Λ-CDM model ($w = -1$). Lines from solid black to dotted light blue delimit the 1- to 5-σ error zones, where σ is the standard deviation.

III.2 Constant quintessence parameter

We now work in a Quintessence-Cold Dark Matter (QCDM) model: the dark energy equation of state is $w = P/\rho$, where P is the pressure of the quintessence fluid, ρ its density, and w is just constrained to be negative. In this section, we work with a time independent w parameter.

III.2.1 Cosmological constant model

I first wrote the code for a ΛCDM cosmology with a varying bias parameter. This reduces the problem to a simple 1D parameter space. For the computation, the idea is to create arrays in ℓ for the fiducial model terms that won't have to be called again, so that we only have to proceed to interpolations at the right ℓ when integrating, making the code run faster.

We show on fig.11 the result for our ADEPT+PLANCK model, with a fiducial value $\bar{b_g} = 1$. The vertical lines delimit the different $n - \sigma$ zones, $n = 1, ..., 5$. We clearly see the gaussian approximation is quite accurate. It may seem that we should be able to get an estimation of the bias parameter to a ~ 0.2 % confidence level. However, we considered here that all the other parameters that constitute our cosmology are known to infinite precision. In fact, they are known to within a given uncertainty, and the true error on the bias parameter is drawn from the width in b_g of the hypervolume that represents the total uncertainty in the parameters space. Let us now see the changes it leads to.

III.2.2 Quintessential model

In our case, we will only consider a 2D uncertainty $b_g - w$ by fixing the other parameters so that the temperature power spectrum, that we hope to constrain with high confidence with next generation observations, is fixed. This can be done by keeping the physical matter density $\Omega_{m,0}\,h^2$, baryonic density $\Omega_{b,0}\,h^2$, and, in the case of a flat Universe, the CMB conformal distance to recombination constant[30]. The first two keep the height of the peaks fixed, whereas the last one keeps their position in ℓ constant[12]. Technically, we first calculate these quantities for our fiducial ΛCDM model, then we change the value of w and look for the $\Omega_{m,0}$ that will recover the fiducial $\eta_{\rm rec}$. Increasing w, and thus increasing the importance of vacuum energy in time, leads to increasing $\Omega_{m,0}$, $\Omega_{b,0}$, and decreasing h: more matter is needed to counterbalance the vacuum energy importance, and as matter dominated until recently, the Hubble constant is lower as matter tends to contract the Universe by decelerating expansion (this effect

[12] In fact, we keep the *angular* diameter distance $d_{\rm ang}(z_{\rm rec}) = \eta(z_{\rm rec})/(1+z_{\rm rec})$, where $z_{\rm rec} = 1100$ is constant, fixed so that the angular size of a fluctuation remains constant.

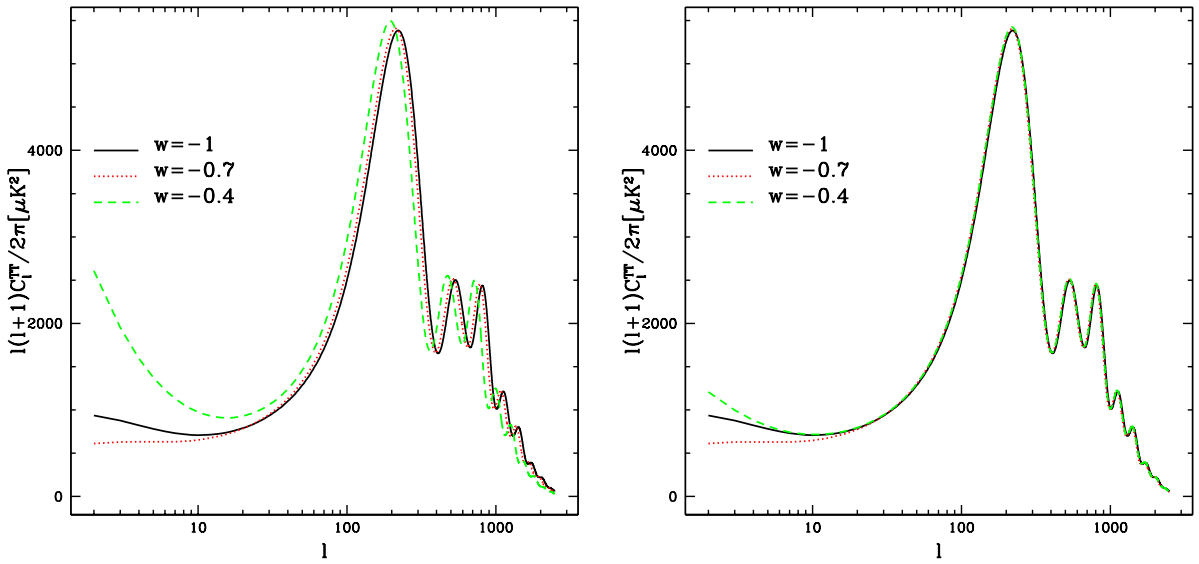

FIG. 12: Temperature angular power spectra obtained by keeping the cosmological constants to their fiducial values (left), and by fixing $\eta_{\rm rec}$, $\Omega_{m,0}h^2$ and $\Omega_{b,0}h^2$, and changing the normalization to match the results at high ℓ's (right). We see that we can conveniently fix the power spectrum on our scales of interest: the small scales of the CMB.

can be seen in **I.1.3**, eq.(11)). Finally, we find the new h with the condition of constant $\Omega_{m,0}\,h^2$, and $\Omega_{b,0}$ is obtained without difficulty with the condition of constant $\Omega_{b,0}\,h^2$. We also have to change the normalization of the power spectrum to match the curves on small scales, however CAMB does that automatically by changing our σ_8.

We compare in fig.12 the non-fixed and fixed power spectra for several values of w. The break of degeneracy that persists for low ℓ's is not of importance, as only high multipoles are of interest to us. Moreover, it should be masked in the end by the cosmic variance.

For the computation of the 2-D joint constraint in the $b_g - w$ plane, we need to include the w parameter where necessary: in the calculation of $\eta(z)$ and in the evolution of the power spectrum (done by CAMB). For each w, we make one call of the power spectra using the fixing technique explained previously, and for each b_g we make the same calculation than before. The former being longer to compute than the latter, it will be done as an external loop, b_g being calculated as an internal loop. We evaluate $\chi^2(b_g, w)$ on a grid of 100×100 points, and the contours are drawn with SM to represent the lines of constant χ^2, in our case $\chi^2 = 1, 2, .., 5$. We show on fig.13 the result for a fiducial model $\bar{b_g} = 1$, $\bar{w} = -1$. We can now see that if we allow w to vary, the error we commit on b_g is of order 1% instead of the 0.2% for w fixed to its fiducial value -1. The shape of the contours can be understood by recalling the effect of quintessence on growth of structure: for $-1 < w < 0$, vacuum energy is more important in the past, and growth of structure is suppressed earlier (recall fig.5). Thus, visible matter has less time to cluster on dark matter overdensities and the bias parameter is lower. The reverse effect is true for $w < -1$.

III.3 Time-varying quintessence parameter: celestine quintessence

Theoretically, quintessence can be time-dependent. The motivation to introduce such a dependence in the dark energy density involves different concepts of high energy field theory we will not get into. This work is part of the Dark Energy Task Force (DETF) report[31]. Here we study a model of quintessence called *celestine quintessence* in which the parametrization of w is very simple[9]:

$$\boxed{w(a) = w_0 + w_a(1-a)} \tag{45}$$

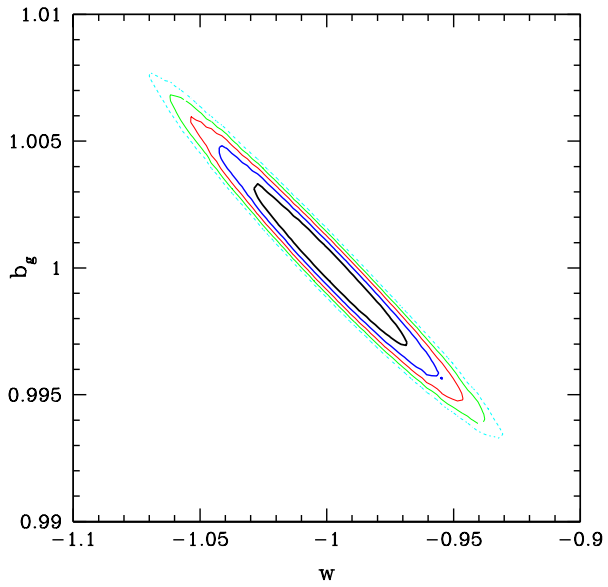

FIG. 13: Contours of constant χ^2 for the joint constraint on the bias parameter b_g and the quintessence parameter w expected for an ADEPT+PLANCK cross-correlation. Solid black to dashed light blue lines delimit the 1- to 5-σ confidence regions.

where a is the scale factor, w_0 the present value of the w parameter, and w_a a new parameter in our model quantifying its time dependence. Our goal is to constrain these two parameters with the same technique as before.

In the case of such a time dependent w parameter, the vacuum energy density reads (see appendix B) :

$$\Omega_Q(a) = \Omega_\Lambda a^{-3\,(1+w_0+w_a)} e^{-3\,w_a(1-a)} \tag{46}$$

This changes our calculation of the conformal distance in eq.(13). We also modify the source code of CAMB by replacing each w by our new parametrization — luckily enough CAMB calls each function at a precise scale factor a —. Finally, we use the same technique than before to fix the temperature angular power spectrum and we take the same fiducial model: $\boxed{\bar{w_0} = 1}$ and $\boxed{\bar{w_a} = 0}$.

To be able to get a 2-D constraint in the $w_0 - w_a$ plane with 3 parameters (b_g,w_0,w_a), we have to *marginalize* over b_g. This process consists in integrating the joint probability, or equivalently — to a proportionality factor — the likelihood function $\mathcal{L}(b_g, w_0, w_a)$, over b_g at fixed (w_0, w_a), which means that we allow b_g to vary freely. In our code, we integrate $e^{-\chi^2(b_g,w_0,w_a)/2}$ over b_g for each point (w_0, w_a) to get the marginalized likelihood, and we obtain the marginalized χ^2 by inverting $\chi^2_{\rm marg} = -2\ln\mathcal{L}_{\rm marg}$. We have an additional constant however, which can be eliminated by substracting the marginalized χ^2 obtained for the fiducial model $\bar{w_0} = 1$, $\bar{w_a} = 0$.

We show on fig.14 the constraints we obtain on these parameters. We can hope to constrain $-1.1 < w_0 < -0.9$ and $-0.4 < w_a < 0.3$ to the 99 % confidence level. The constraint on the time dependence w_a of the dark energy equation of state corresponds to the optimistic previsions of the report of the DETF. As their estimations are given for *combined* techniques (study of Supernovae, galaxy clusters...), this is a very encouraging result for weak lensing, which is only a single technique.

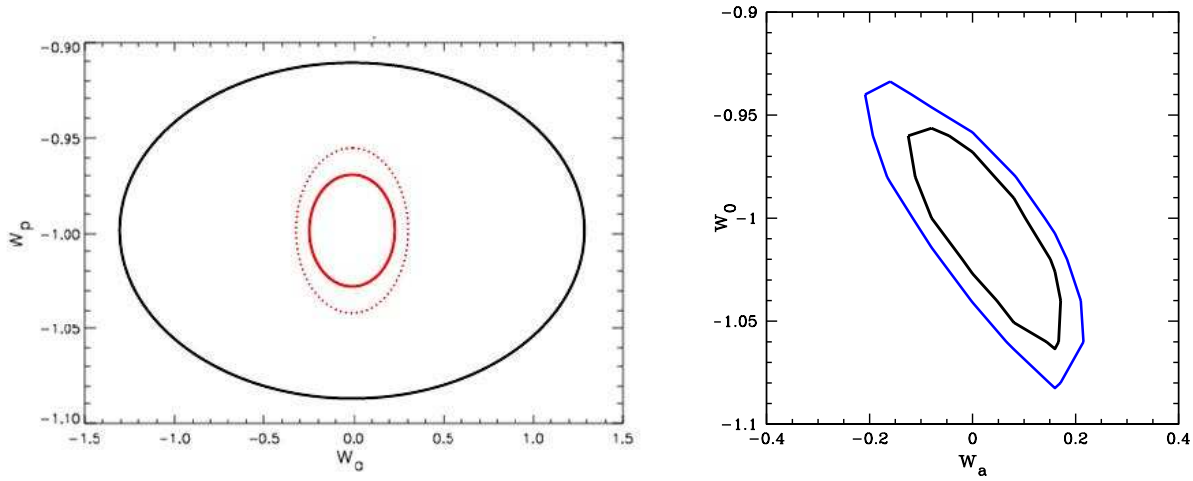

FIG. 14: On the left: 2-σ confidence contours for the quintessence parameters w_0 and w_a expected for upcoming observations, as presented in the report of the DETF.[31] The outer black line is the constraint we hope to get from ongoing projects that are relevant to dark energy, and inner red contours are pessimistic (dotted line) and optimistic (solid line) expectations for future missions. On the right, our contours for an ADEPT+PLANCK cross-correlation. The black line is the 1-σ contour and the blue line the 2-σ one. In both cases, the fiducial model is $\bar{w_0} = 1$, $\bar{w_a} = 0$.

IV The next step

Now that we have written our codes, it would be interesting to study some features.

- First, we made an approximation in eq.(44). The whole, non-approximated χ^2 reads:

$$\chi^2(b_g, w_0, w_a) = 2 f_{\rm sky} \int \ell d\ell \left(\frac{\left[C_\ell^{\tilde{\Sigma}_g - \kappa}(b_g, w_0, w_a) - C_\ell^{\tilde{\Sigma}_g - \kappa} \right]^2}{\left(C_\ell^{\kappa\kappa} + N_\ell^{\kappa\kappa} \right) C_\ell^{\tilde{\Sigma}_g - \kappa} + \left(C_\ell^{\tilde{\Sigma}_g - \kappa} \right)^2} + \sum_{i = \tilde{\Sigma}_g, \kappa} \frac{\left[C_\ell^{i-i}(b_g, w_0, w_a) - C_\ell^{i-i} \right]^2}{\left(N_\ell^{i-i} + C_\ell^{i-i} \right)^2} \right)$$

  We actually thought the signal terms in the denominators as well as the convergence term could be neglected. Adding the signal terms in our calculation tends to decrease χ^2 and broaden the constraint (this is a cosmic variance noise), while adding the convergence tends to increase it and make the constraints narrower as we get more information on the power spectrum through κ. There is a balance between the two effects. It seems that the constraints are in the end poorer with this full χ^2. The next step would thus be to include the full χ^2 in our codes and calculate the new, non approximated constraints.

- Then, we studied the simple case of a constant, redshift independent bias parameter b_g. However, the growth of structure depends on redshift and galaxies clump more and more on dark matter over-densities as time goes on: they become better tracers of the underlying dark matter fluctuations and the bias parameter should thus increase with cosmic time (or decrease with redshift). To conduct a more realistic study, we could divide our model redshift distribution in different redshift bins, and take for each bin a different fiducial bias parameter. As each bin gives some information on the growth of structure at a specific time, the combination of the different studies should allow us to improve the constraints on dark matter and dark energy.

- Finally, combining this study with other techniques could improve this constraint (see fig.15).

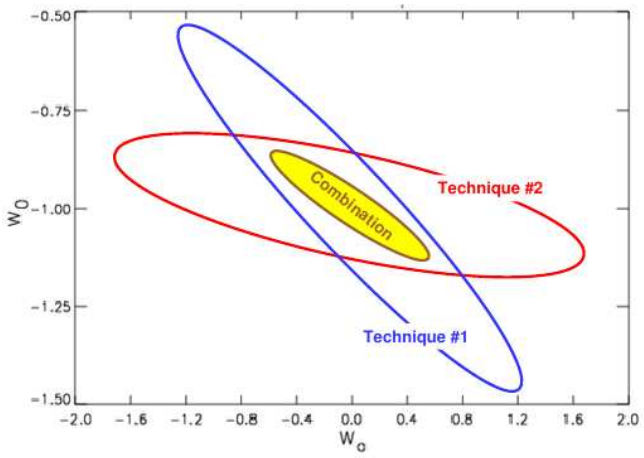

FIG. 15: Illustration of the power of combining techniques. Technique #1 and technique #2 have roughly the same $2-\sigma$ confidence contour (blue and red lines). However, when combined, the resulting $2-\sigma$ contour is substantially improved. Our cross-correlation is a single technique. However, we could think of combining with other independent techniques. Figure found in the Report of the DETF.[31]

Conclusion

With new astrophysical observations bringing more information with less noise comes the possibility to know the different cosmological parameters to a never reached precision. Their knowledge brings us the understanding of our cosmological history, our future, our Universe. To extract the information from our different observations, one can reveal cunning and use the underlying correlations. Our case of interest is the use of both visible matter fluctuations obtained through galaxy surveys and dark matter fluctuations guessed through the CMB convergence. The cross-correlation of these signals should give us a precise insight on the galaxy bias parameter b_g, parameter describing the way visible and dark matters follow each other. Moreover, the clustering information we would get on visible matter is an indicator of the growth of primordial density fluctuations in the Universe, their evolution and their suppression, all of which can be drawn from the behavior of dark energy, a mysterious fluid with equation of state $w = P/\rho < 0$. These two parameters are correlated, since a high clustering, or high b_g, reveals a late growth suppression, or low w.

The calculation of a signal-to-noise showed the excellent expectations one could have by using upcoming surveys such as PLANCK for the CMB and ADEPT or the ESA Cosmic Vision Program for the galaxy redshift survey. More precision can even be obtained through the use of a convenient filter applied on the visible matter fluctuations to keep the best signal-to-noise regions. To quantify these expectations, the χ^2 method reveals a pertinent approach to have a theoretical prediction on the parameters estimation. By building joint constraints, one can see the degeneracies between parameters around fiducial values and evaluate the errors committed on their estimations for given experiments. Considering the CMB we observe is known with enough confidence so that we consider it can be fixed to its best-fit value, we constrained the bias parameter b_g and the dark energy parameter w. The degeneracy between the two appears clearly, and the error estimations of 1% for b_g and 10% for w turns out to be a considerable improvement on the actual ones. However, a time dependence of the dark energy, by modifying the growth of structure and thus the matter power spectrum, would leave a trace in what we observe that can be constrained as well. Adopting the simple model of celestine Quintessence, we showed that constraints are quite comparable to the expectations of the Dark Energy Task Force, and could even be improved by combining with different techniques. Finally, dividing the distribution into redshift bins and introducing a time-varying bias parameter would be the next steps in our study, another one on the path to more precise cosmological parameters constraints.

Appendix A

Origin of cosmological redshift

In this section, we find the relation between the cosmological redshift and the scale factor. Let us set up the situation. We consider an object that is at a fixed comoving distance from the observer, and we consider two successive wave crests emitted by the object[1]. It is subject to Doppler shift due to the expansion of the Universe. Let the wavelength at emission be λ_e, and the observed wavelength be λ_0. The first crest is emitted at physical time t_e and observed at physical time t_0. The second is emitted at time $t_e + \lambda_e$ and observed at time $t_0 + \lambda_0$ (with the convention $c = 1$). Both wave crests travel the same fixed *comoving* distance, so they take the same amount of *conformal* time (which equals the comoving distance for $c = 1$) to make the trip:

$$\int_{t_e}^{t_0} \frac{dt}{a(t)} = \int_{t_e+\lambda_e}^{t_0+\lambda_0} \frac{dt}{a(t)} \tag{A.1}$$

Then, adding the quantity $\int_{t_0}^{t_e+\lambda_e} \frac{dt}{a(t)}$, which is the conformal time during which both crests are "in flight", we get:

$$\int_{t_e}^{t_e+\lambda_e} \frac{dt}{a(t)} = \int_{t_0}^{t_0+\lambda_0} \frac{dt}{a(t)} \tag{A.2}$$

Hopefully, we find that the conformal period of the radiation is the same at the emitter and the observer. We then make the approximation that the scale factor doesn't change appreciably over the course of either integral in the above expression[2], so that equation A.2 rewrites

$$\frac{1}{a(t_e)} \int_{t_e}^{t_e+\lambda_e} dt = \frac{1}{a(t_0)} \int_{t_0}^{t_0+\lambda_0} dt \tag{A.3}$$

This simply yields

$$\frac{\lambda_0}{\lambda_e} = \frac{a(t_0)}{a(t_e)} \tag{A.4}$$

Using $a(t_0) = 1$ and $z = \frac{\lambda_0 - \lambda_e}{\lambda_e}$, we get the relationship between reshift and scale factor at physical time t:

$$\boxed{z(t) = \frac{1}{a(t)} - 1} \iff \boxed{a(t) = \frac{1}{1 + z(t)}} \tag{A.5}$$

[1] This explanation is adapted from Ryden (2003), section 3.4

[2] This is justified because the period of a photon is of order 10^{-15} seconds while the time it takes the Universe to expand appreciably is $H(t)^{-1} \sim 10^{10}$ years.

Following is an example of cosmological redshift in the optical spectrum of a supercluster of distant galaxies [3]:

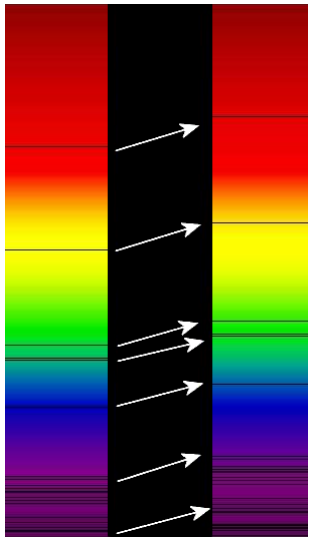

FIG. 1: Redshift of spectral lines in the optical spectrum of a supercluster of distant galaxies (right), as compared with that of the Sun (left). Wavelength increases up towards the red and beyond as the supercluster recesses from us.

[3] Figure found on `http://en.wikipedia.org/wiki/Redshift`

Appendix B

Friedmann equations

Friedmann equations are derived from the energy tensor relations of General Relativity for an isotropic and homogeneous (in a word, cosmological) Universe. The main equation is:

$$\boxed{H(a)^2 = \left(\frac{\dot{a}}{a}\right)^2 = \frac{8\pi}{3}\rho(a)} \tag{B.1}$$

where we used the convention $G = c = 1$ (where G is Newton's gravitational constant), $H(a)$ is the Hubble constant at time t corresponding to a scale factor $a(t)$, and $\rho(a)$ is the total energy density in the Universe at that time. It can be decomposed into four different components: ρ_r for radiation and relativistic matter (accounting for dark matter as well, the Hot Dark Matter or HDM), ρ_m for non relativistic matter and dark matter (Cold Dark Matter or CDM), ρ_k for the curvature of the Universe, and ρ_Λ for the cosmological constant or vacuum energy density. One can also derive a conservation condition for each component i:

$$\dot{\rho}_i/\rho_i = -3H(a)(1 + P_i/\rho_i) = -3H(a)[1 + w_i] \tag{B.2}$$

where P_i is the pressure of component i, and $w_i = P_i/\rho_i$ its equation of state. Since $H(a) = \dot{a}/a$, we can write eq.(B.2) as $\log \rho_i/\rho_{i,0} = -3\int_1^a \mathrm{d}\log a'[1 + w_i]$. In the simple case of a constant equation of state, this yields

$$\rho_i = \rho_{i,0}\, a^{-3[1+w_i]}$$

where $\rho_{i,0}$ is the present value of the component i energy density. Let us work out the dynamic of these components of ρ. For ρ_m, the energy density is mainly the matter rest mass, which remains constant as the Universe expands, times a physical (not comoving) number density, therefore scaling as a (physical length)$^{-3}$: $\rho_m \propto a^{-3}$, so that $\boxed{w_m = 0}$. In the radiative case ρ_r, the energy density must take into account the frequency (thus momentum) redshift experienced during expansion — $h\nu \propto (1+z)$ —, yielding another factor a^{-1} in the relation: $\rho_r \propto a^{-4}$, giving $\boxed{w_r = 1/3}$. As the radiation density also scales as T^4, where T is the temperature, we find another important result:

$$\boxed{T(z) \propto (1 + z)} \tag{B.3}$$

For the curvature of the Universe, the relation is $\rho_k = -k/a^2$, where k is -1 for an open Universe, 0 for a flat one, and $+1$ for an open one, so that $\boxed{w_k = -1/3}$. This energy density, which scales as a surface density, can be seen as a surface tension. Finally, the last term ρ_Λ is the most mysterious one. It is thought to be a constant vacuum energy density, with equation of state $\boxed{w_\Lambda = -1}$. However, it could be time varying with equation of state $w(a)$, in which case we refer to it as Quintessence with energy density ρ_Q. In the case of the so-called *celestine Quintessence*, $w(a) = w_0 + (1 - a)w_a$, where w_0 and w_a are constant parameters, and the energy density evolves as

$$\begin{aligned}\rho_Q &= \rho_{Q,0}\,\exp\left(-3\int_1^a d\log a'[1+w_0+(1-a)w_a]\right)\\ &= \rho_{Q,0}\,a^{-3\,(1+w_0+w_a)}\,e^{-3\,w_a(1-a)}\end{aligned} \tag{B.4}$$

Defining the critical density to be $\rho_c = 3H_0^2/8\pi$ — the present total energy density, $\rho_c = 9.4 \times 10^{-30}$ g.cm^{-3}—, and using the fact that $a_0 = 1$, one can finally define the reduced quantities $\Omega_i \equiv \rho_i/\rho_c$, with present values $\Omega_{i,0}$, and rewrite equation (B.1) as

$$\boxed{H^2(a) = {H_0}^2\left(\frac{\Omega_{r,0}}{a^4}+\frac{\Omega_{m,0}}{a^3}+\frac{\Omega_{k,0}}{a^2}+\frac{\Omega_{Q,0}}{a^{3\,(1+w_0+w_a)}\,e^{3\,w_a(1-a)}}\right)} \tag{B.5}$$

We recover for $w_0 = -1$, $w_a = 0$ the case of the cosmological constant presented in eq.(B.1).

Appendix C

The CMB fluctuations

In the current paradigm of cosmology, the initial fluctuations in the gravitational field are the result of quantum fluctuations, which raised on macroscopic scales during an *inflationary epoch* in the very early Universe between 10^{-37} and 10^{-35} seconds, increasing dramatically the scale factor of approximately 60 e-folds ($\sim 10^{26}$ times bigger than before inflation). During the radiation era, these fluctuations couldn't grow because of the predominant photons pressure. But after matter energy density began to dominate (*i.e.* after matter-radiation equality, see fig.1), these initial fluctuations began to grow.

In the tightly coupled fluid of baryons and photons composing the Universe by that time, two main tendancies tend to increase fluctuations. The first one is the gravitationnal pull which tends to attract more matter in over-dense regions, and the other one is the photons pressure, which balances the first effect. As a region becomes *denser* because of gravitation, it will also become *hotter* due to the increase number density of photons (which follow the variation of matter density as they are tightly coupled with baryons), and thus the pressure will increase as well. For under-dense regions, we would have the inverse effect. This balance creates density oscillations in the photon-baryon plasma where initial fluctuations have grown, and their importance depends on the different cosmological parameters. The CMB is a "snapshot" of these oscillations at recombination time, showing us more particularly regions where the density is at its maximum (hot spot) or minimum (cold spot), and regions where it is at half oscillation (almost no fluctuation in temperature). Moreover, the scale of these regions depends on the *sound horizon* at recombination, which is the comoving distance a sound wave can have traveled since matter-radiation equality, and under which causality is respected and information can have travelled to create a coherent oscillation. What we see, then, is a *fundamental* on this sound horizon scale, and its *harmonics* on scales below: indeed, only scales which vary by an integer factor with respect to the fundamental scale have had time to oscillate a periodic number of times, so that they are at one particular stage of oscillation when photons decoupled: maximum, minimum or half oscilation.

We show in fig.1 an example of temperature angular power spectrum with three distinct regions. The Sachs-Wolfe plateau is a very large scale region above the sound horizon causal limit, where only variations in gravitational field can affect the temperature fluctuations through photons gravitational redshift. Since the calculation give a spectrum $\propto \ell^{-2}$ for this effect, the convention is to write $\ell(\ell+1)C_\ell^{TT}$, so that it flattens the beginning of the curve. The multipole $\ell \simeq 200$ corresponds to the first peak: it is the scale at which we see the sound horizon today. Under this scale are the acoustic peaks (traditionnaly referred as *Doppler peaks*). The small-scale damping, called *Silk damping* or *diffusion damping*, is caused by the finite thickness of the Last Scattering Surface — in other terms, decoupling didn't occur immediately —, so that we average over a finite time during which small-scale perturbations are consistently changing because of photons diffusion.

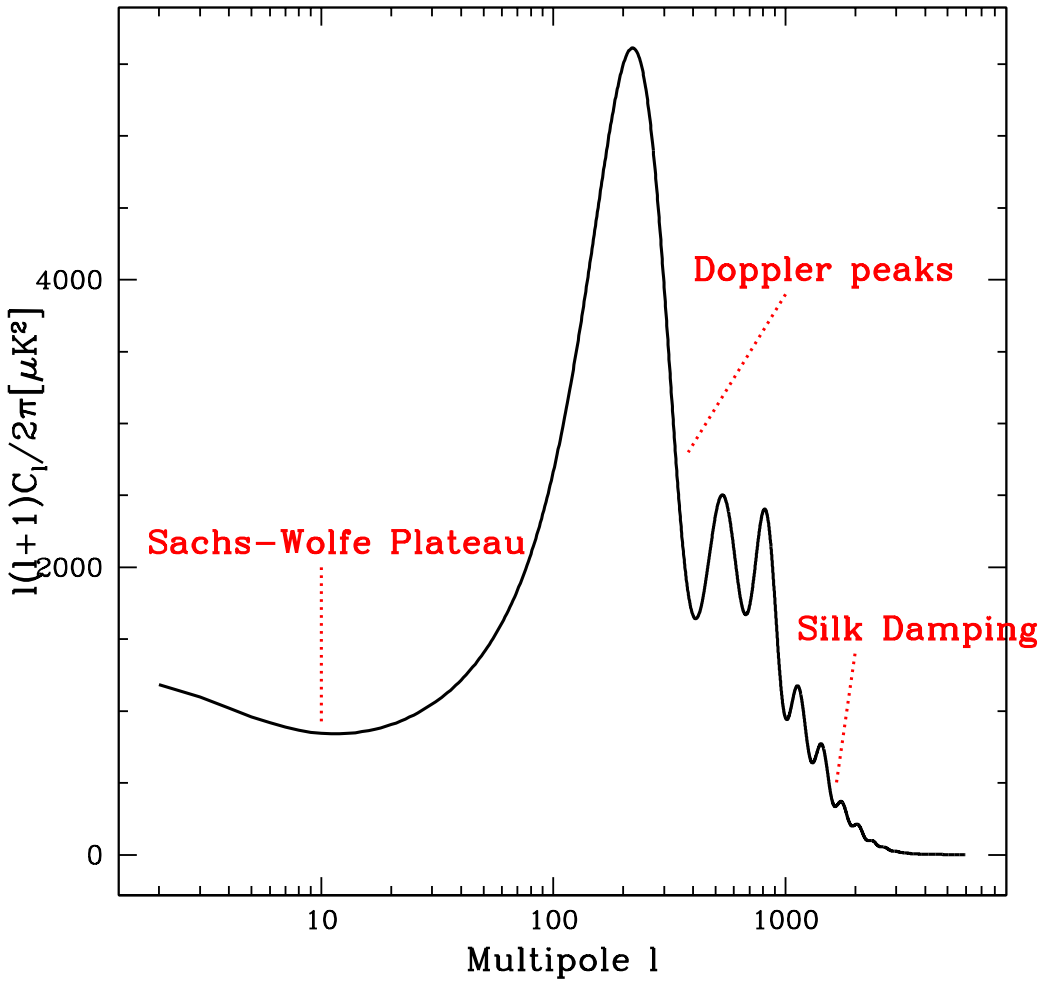

FIG. 1: Temperature angular power spectrum as a function of multipole. Three distinct behaviors can be seen, depending on the scale. Computed with CAMB for my fiducial cosmology.

Appendix D

The cross-correlation formalism

I An exact calculation

In this part, we will separate the time dependance from the evolved power spectrum presented in **I.2** by introducing explicitly the growth factor $D(\eta)$:

$$\delta(\vec{x},\eta) = \frac{D(\eta)}{D(0)}\delta(\vec{x},0) \tag{D.1}$$

Let us now think of $D(\eta)$ as the growth factor normalized to its present value $\frac{D(\eta)}{D(0)} \to D(\eta)$. The non evolved, present time power spectrum of the correlations of dark matter density fluctuation is defined through:

$$\langle \delta(\vec{k},0)\, \delta^*(\vec{k}',0)\rangle_{\text{galaxies}} = P(k)\; \delta_{Dirac}(\vec{k}-\vec{k}') \tag{D.2}$$

The average is made on the distribution of galaxies. Using this relation, and the equations (28) and (30), we calculate:

$$\begin{aligned}\langle\, \Sigma_g(\hat{n})\kappa_{\text{CMB}}(\hat{m})^*\,\rangle_{\text{galaxies}} = \frac{3{H_0}^2\Omega_{m,0}}{2}\int_0^{\eta_{\text{rec}}} d\eta\, b_g W_\eta(\eta) D(\eta) \\ \times \int_0^{\eta_{\text{rec}}} d\eta' \frac{(\eta_{\text{rec}}-\eta')}{\eta_{\text{rec}}}\,\frac{\eta'}{a(\eta')}\,D(\eta')\int \frac{k^2 dk}{(2\pi)^3}P(k)\int d\Omega_k e^{i\vec{k}.\hat{n}\eta}e^{-i\vec{k}.\hat{m}\eta'}\end{aligned} \tag{D.3}$$

Then, using the relation

$$\int d\Omega_k e^{i\vec{k}.\vec{n}\eta}e^{-i\vec{k}.\vec{m}\eta'} = 4\pi\sum_\ell (2\ell+1) j_\ell(k\eta) j_\ell(k\eta') P_\ell(\vec{m}.\vec{n}) \tag{D.4}$$

where j_ℓ is the ℓth spherical Bessel function and P_ℓ the ℓth Legender polynome, we find

$$\langle\, \Sigma_g(\hat{n})\kappa_{\text{CMB}}(\hat{m})^*\,\rangle_{\text{galaxies}} = \sum_\ell \frac{2\ell+1}{4\pi} C_\ell^{\Sigma_g-\kappa} P_\ell(\vec{m}.\vec{n}) \tag{D.5}$$

where

$$\boxed{C_\ell^{\Sigma_g-\kappa} = \frac{2}{\pi}\int k^2 dk\, w_\ell^{\Sigma_g}(k) w_\ell^{\kappa}(k)} \tag{D.6}$$

with

$$w_\ell^{\Sigma_g}(k) = \int_0^{\eta_{\text{rec}}} d\eta\, b_g W_\eta(\eta)\sqrt{P(k)} D(\eta) j_\ell(k\eta) \tag{D.7}$$

and

$$w_\ell^\kappa(k) = \left(\frac{3{H_0}^2\Omega_{m,0}}{2}\right)\int_0^{\eta_{\rm rec}} d\eta \frac{(\eta_{\rm rec}-\eta)}{\eta_{\rm rec}}\,\frac{\eta}{a(\eta)}\,\sqrt{P(k)}D(\eta)j_\ell(k\eta) \tag{D.8}$$

Following the same path, one can calculate the number count and convergence autocorrelation:

$$\boxed{C_\ell^{\Sigma_g-\Sigma_g} = \frac{2}{\pi}\int k^2dk\left[w_\ell^{\Sigma_g}(k)\right]^2} \tag{D.9}$$

and

$$\boxed{C_\ell^{\kappa-\kappa} = \frac{2}{\pi}\int k^2dk\left[w_\ell^{\kappa}(k)\right]^2} \tag{D.10}$$

We can now see that the evolved power spectrum is naturally introduced by the replacement $P(k)D(\eta)^2 \to P(k, a(\eta))$.

II The Limber approximation

Here we work out the calculation of the Limber approximation made in **II.2.2**, where we used:

$$j_\ell(k\eta) \simeq \sqrt{\frac{\pi}{2\ell}}\delta_D(\ell+1/2-k\eta) \tag{D.11}$$

We first note that

$$\int d\eta\, G(\eta)\delta_D(\ell-k\eta) = \frac{1}{|k|}G\left(\frac{\ell}{k}\right) \tag{D.12}$$

where G is a given function of conformal time. Let us now derive the correlation functions in this approximation. If we expand $w_\ell^X(k)$ as

$$w_\ell^X(k) = \int d\eta\, G_\ell^X(k,\eta)\, j_\ell(k\eta) \tag{D.13}$$

we then want to find the Limber approximation for C_ℓ^{X-Y}:

$$\begin{aligned} C_\ell^{X-Y} &= \frac{2}{\pi}\int k^2dk\, w_\ell^X(k)w_\ell^Y(k) \\ &= \frac{2}{\pi}\int k^2dk\int d\eta\int d\eta' G_\ell^X(k,\eta)G_\ell^Y(k,\eta')j_\ell(k\eta)j_\ell(k\eta') \\ &= \frac{1}{\ell}\int_{\frac{\ell}{\tau_0}}^{+\infty} dk\, G_\ell^X\left(k,\frac{\ell}{k}\right)G_\ell^Y\left(k,\frac{\ell}{k}\right) \\ &= \int_0^{\tau_0}\frac{d\eta}{\eta^2}\,G_\ell^X\left(\frac{\ell}{\eta},\eta\right)G_\ell^Y\left(\frac{\ell}{\eta},\eta\right) \end{aligned} \tag{D.14}$$

where we made in the last line the change of variable $k \to \frac{\ell}{\eta}$. We then simply apply in eq.(31) to get eq.(34).

Appendix E

The filter

We look for the filter $w_\ell(k,\eta)$ that will maximize our signal-to-noise. In the processus of maximization, we make use of the functional derivative theory. The functional derivative of a function $F[f(x)]$ is defined as follow:

$$\frac{\delta F[f(x)]}{\delta f(y)} = \lim_{\epsilon \to 0} \frac{F[f(x) + \epsilon \delta_D(x-y)] - F[f(x)]}{\epsilon} \tag{E.1}$$

so that the functional derivatives of the filtered functions $C_\ell^{\tilde{\Sigma}_i - \kappa}[w_\ell(k',\eta')]$ and $C_\ell^{\tilde{\Sigma}_i - \tilde{\Sigma}_i}[w_\ell(k',\eta')]$ with respect to the filter are just:

$$\begin{aligned}
\frac{\delta C_\ell^{\tilde{\Sigma}_g - \kappa}[w_\ell(\eta')]}{\delta w_\ell(\eta)} &= \left(\frac{3{H_0}^2\Omega_{m,0}}{2}\right) \frac{1}{\eta} \left[\frac{\eta_{\rm rec} - \eta}{a(\eta)\,\eta_{\rm rec}}\right] [b_g W_\eta(\eta)]\, P(\ell/\eta, a) \\
\frac{\delta C_\ell^{\tilde{\Sigma}_g - \tilde{\Sigma}_g}[w_\ell(\eta')]}{\delta w_\ell(\eta)} &= \frac{2{W_\eta(\eta)}^2}{\eta^2} {b_g}^2 P(\ell/\eta, a)\, w_\ell(\ell/\eta, \eta) \\
\frac{\delta N_\ell^{\tilde{\Sigma}_g - \tilde{\Sigma}_g}[w_\ell(\eta')]}{\delta w_\ell(\eta)} &= \frac{2{W_\eta(\eta)}^2}{\eta^2} {n_g(\eta)}^{-1}\, w_\ell(\ell/\eta, \eta)
\end{aligned} \tag{E.2}$$

As the convergence auto-correlation doesn't depend upon the filter, it is possible to have it vanished by taking the logarithmic functional derivative of the filtered signal-to-noise given in eq.(39) with respect to w_ℓ. Setting to 0 yields:

$$\frac{2}{C_\ell^{\tilde{\Sigma}_g - \kappa}} \frac{\delta C_\ell^{\tilde{\Sigma}_g - \kappa}}{\delta w_\ell(\eta)} = \frac{1}{C_\ell^{\tilde{\Sigma}_g - \tilde{\Sigma}_g} + N_\ell^{\tilde{\Sigma}_g - \tilde{\Sigma}_g}} \frac{\delta (C_\ell^{\tilde{\Sigma}_g - \tilde{\Sigma}_g} + N_\ell^{\tilde{\Sigma}_g - \tilde{\Sigma}_g})}{\delta w_\ell} \tag{E.3}$$

which writes explicitly

$$\begin{aligned}
&\frac{2\left(\frac{3{H_0}^2\Omega_{m,0}}{2}\right)\frac{1}{\eta}\left[\frac{\eta_{\rm rec}-\eta}{a(\eta)\,\eta_{\rm rec}}\right] b_g W_\eta(\eta) P(\ell/\eta, a)}{\int d\eta \left(\frac{3{H_0}^2\Omega_{m,0}}{2}\right)\frac{1}{\eta}\left[\frac{\eta_{\rm rec}-\eta}{a(\eta)\,\eta_{\rm rec}}\right] b_g W_\eta(\eta) P(\ell/\eta, a)\, w_\ell(\ell/\eta,\eta)} = \\
&\qquad\qquad \frac{\frac{2}{\eta^2}{W_\eta(\eta)}^2 \left[{b_g}^2 P(\ell/\eta, a) + \frac{1}{n_g(\eta)}\right] w_\ell(\ell/\eta,\eta)}{\int d\eta\, \frac{1}{\eta^2}{W_\eta(\eta)}^2 \left[{b_g}^2 P(\ell/\eta, a) + \frac{1}{n_g(\eta)}\right] w_\ell(\ell/\eta,\eta)^2}
\end{aligned} \tag{E.4}$$

We finally find the convenient weight by equaling numerators (or denominators), yielding

$$\boxed{w_\ell(k = \ell/\eta, \eta) = \left(\frac{3{H_0}^2\Omega_{m,0}}{2}\right)\left[\frac{\eta_{\rm rec}-\eta}{a(\eta)\,\eta_{\rm rec}}\right] \frac{\eta}{b_g W_\eta(\eta)} \left(\frac{{b_g}^2 P(\ell/\eta, a)}{{b_g}^2 P(\ell/\eta, a) + \frac{1}{n_g(\eta)}}\right)} \tag{E.5}$$

Index

Bibliography

[1] E. Hubble. *Proceedings of the National Academy of Sciences*, **15**, 168, (1929).

[2] F. Zwicky. *Helvetica Physica Acta*, **6**, 110, (1933).

[3] A. G. Riess, A. V. Filippenko, P. Challis, A. Clocchiatti, A. Diercks, P. M. Garnavich, R. L. Gilliland, C. J. Hogan, S. Jha, R. P. Kirshner, B. Leibundgut, M. M. Phillips, D. Reiss, B. P. Schmidt, R. A. Schommer, R. C. Smith, J. Spyromilio, C. Stubbs, N. B. Suntzeff, and J. Tonry. *Astrophys. J.*, **116**, 1009, (1998), arXiv:astro-ph/9805201.

[4] S. Perlmutter, G. Aldering, G. Goldhaber, R. A. Knop, P. Nugent, P. G. Castro, S. Deustua, S. Fabbro, A. Goobar, D. E. Groom, I. M. Hook, A. G. Kim, M. Y. Kim, J. C. Lee, N. J. Nunes, R. Pain, C. R. Pennypacker, R. Quimby, C. Lidman, R. S. Ellis, M. Irwin, R. G. McMahon, P. Ruiz-Lapuente, N. Walton, B. Schaefer, B. J. Boyle, A. V. Filippenko, T. Matheson, A. S. Fruchter, N. Panagia, H. J. M. Newberg, W. J. Couch, and The Supernova Cosmology Project. *Astrophys. J.*, **517**, 565, (1999), arXiv:astro-ph/9812133.

[5] R. R. Caldwell, R. Dave, and P. J. Steinhardt. *Phys. Rev. Lett.*, **80**, 1582, (1998), arXiv:astro-ph/9708069.

[6] A. A. Penzias and R. W. Wilson. *Astrophys. J.*, **142**, 419, (1965).

[7] D. N. Spergel, R. Bean, O. Doré, M. R. Nolta, C. L. Bennett, J. Dunkley, G. Hinshaw, N. Jarosik, E. Komatsu, L. Page, H. V. Peiris, L. Verde, M. Halpern, R. S. Hill, A. Kogut, M. Limon, S. S. Meyer, N. Odegard, G. S. Tucker, J. L. Weiland, E. Wollack, and E. L. Wright. *Astrophys. J. Sup.*, **170**, 377, (2007), arXiv:astro-ph/0603449.

[8] H. V. Peiris and D. N. Spergel. *Astrophys. J.*, **540**, 605, (2000), astro-ph/0001393.

[9] E. V. Linder. *Phys. Rev. Lett.*, **90**, 091301, (2003), arXiv:astro-ph/0208512.

[10] J. C. Mather, D. J. Fixsen, R. A. Shafer, C. Mosier, and D. T. Wilkinson. *Astrophys. J.*, **512**, 511, (1999), arXiv:astro-ph/9810373.

[11] Found at : `http://upload.wikimedia.org/wikipedia/commons/a/a5/WMAP.jpg`.

[12] E. Komatsu, A. Kogut, M. R. Nolta, C. L. Bennett, M. Halpern, G. Hinshaw, N. Jarosik, M. Limon, S. S. Meyer, L. Page, D. N. Spergel, G. S. Tucker, L. Verde, E. Wollack, and E. L. Wright. *Astrophys. J. Sup.*, **148**, 119, (2003), arXiv:astro-ph/0302223.

[13] L. Knox. *Phys. Rev. D*, **52**, 4307, (1995), arXiv:astro-ph/9504054.

[14] W. Hu. *Astrophys. J. Lett.*, **557**, L79, (2001), arXiv:astro-ph/0105424.

[15] S. Dodelson. *Modern Cosmology*. Academic Press, Amsterdam, Netherlands, (2003).

[16] All the best-fit values for different combinations can be found at : `http://lambda.gsfc.nasa.gov/product/map/current/params/lcdm_wmap_bao.cfm`.

[17] For more information, see : http://sci.esa.int/science-e/www/object/index.cfm?fobjectid=34730&fbodylongid=1595.

[18] A. Lewis and A. Challinor. Code for Anisotropies in the Microwave Background, (2006). See http://camb.info/. This code is based on CMBFAST by U. Seljak & M. Zaldarriaga.

[19] P. Schneider. *ArXiv Astrophysics e-prints*, (2003), astro-ph/0306465.

[20] W. Hu. CMB Anisotropies : A Decadal Survey. In *Birth and Evolution of the Universe*, to be published.

[21] N. Afshordi, Y.-S. Loh, and M. A. Strauss. *Phys. Rev. D*, **69**, 083524, (2004), astro-ph/0308260.

[22] W. Hu. *Physical Review D*, **62**, 043007, (2000) arXiv:astro-ph/0001303.

[23] M. Loverde, L. Hui, and E. Gaztañaga. *Physical Review D*, **75**, 043519, (2007).

[24] Advanced Dark Energy Telescope (ADEPT), see http://www.jhu.edu/news_info/news/home06/aug06/adept.html.

[25] Large Synoptic Survey Telescope (LSST), see http://www.lsst.org.

[26] European Space Agency (ESA) Cosmic Vision Program, see http://www.esa.int/esaSC/SEMA7J2IU7E_index_0.html.

[27] Sloan Digital Sky Survey (SDSS), see http://www.sdss.org/.

[28] Wide Field Fiber Multi-Object Spectrograph (WFMOS), see http://www.gemini.edu/index.php?option=content&task=view&id=145.

[29] The Hobby-Eberly Telescope Dark Energy Experiment (HETDEX), see http://www.as.utexas.edu/hetdex/.

[30] A. Melchiorri, L. Mersini, C. J. Ödman, and M. Trodden. *Phys. Rev. D*, **68**, 043509, (2003), arXiv:astro-ph/0211522.

[31] A. Albrecht, G. Bernstein, R. Cahn, W. L. Freedman, J. Hewitt, W. Hu, J. Huth, M. Kamionkowski, E. W. Kolb, L. Knox, J. C. Mather, S. Staggs, and N. B. Suntzeff. Report of the Dark Energy Task Force. *ArXiv Astrophysics e-prints*, (2006), astro-ph/0609591.